NTNU – Trondheim
Norwegian University of
Science and Technology

Aeroacoustics in a Flow Pipe with a small, variable-length Cavity

Anders Bakke Krogvig

Master of Science in Electronics
Submission date: June 2012
Supervisor: Ulf R Kristiansen, IET

Norwegian University of Science and Technology
Department of Electronics and Telecommunications

Abstract

Pipes with corrugations or cavities are used in a wide variety of applications. In recent years the natural gas industry has experienced "singing" risers, where pipes transporting natural gas excite loud whistling sounds limiting the flow rate of which the gas can be transported. There has been a number of publications regarding this phenomenon, investigating corrugated pipes and pipes with one or more cavities. In this thesis the most basic situation will be studied; A smooth pipe with a single small cavity. This is studied by simulations and experiments. The effects of changing the length of the cavity, and the pipe section between the inlet and the cavity is investigated. The simulations were conducted in Palabos, a Lattice Boltzmann solver which proves to be a promising piece of software for acoustic simulations. The experiments were conduced using a metal pipe with variable inlet and cavity length. Initial vortices created at the inlet are amplified in the cavity by a cavity flow. The results strongly suggest that these inlet vortices are essential for the excitation of whistling sounds. The number of vortices traveling across a cavity at the time is called a hydrodynamic mode. When the frequency of vortices crossing a cavity coincides with an acoustic pipe mode, a whistling sound close to this frequency is excited. Cancellation of the whistling sound with an added cancellation frequency is possible for certain cavity and inlet lengths.

Sammendrag

Strømningsrør med innvendige rugler eller kaviteter har mange bruksområder. De siste årene har naturgassindustrien hatt problemer med at noen av rørene som frakter naturgass opp til plattformene har eksitert en sterk lyd, også kaldt "hyletoner". Disse sterke hyletonene kan elimineres ved at hastigheten på gassen gjennom røret reduseres, men dette er ikke en god løsning fordi hastigheten ofte må være veldig lav. En rekke publikasjoner som omhandler dette fysiske fenomenet er gitt ut, både om ruglerør og rør med en kavitet. I denne oppgaven ble et veldig enkelt tilfelle undersøkt; Et vanlig rør med én kavitet. Denne situasjonen ble studert ved hjelp av simulering og eksperiment. Simuleringene ble utført med Palabos, et dataprogram som viser seg å være et lovende simuleringsvektøy for akustikk i strømningssammenheng. Effekter av å endre kavitetslengden, og inntakslengden mellom rørets inntak og kaviteten ble undersøkt. Strømningsvirvler som genereres ved inntaket blir forsterket i kaviteten, av en kavitetsstrømning. Resultatene tyder på at disse inntaksvirvelene er essensielle for at hyletoner skal kunne eksiteres. Antallet strømningsvirvler som er i en kavitet om gangen kalles en hydrodynamisk mode. Når frekvensen av virvler som krysser kaviteten sammenfaller med en akustisk mode, vil en hyletone med tilsvarende frekvens kunne eksiteres. Kansellering av hyletoner ved bruk av en annen, tilført frekvens, er mulig for enkelte kavitet- og inntakslengder.

Contents

List of Figures

List of Tables

Chapter 1

Introduction

Pipes with cavities, or corrugated pipes, are used when a pipe needs to be flexible. This is the case for example for vacuum cleaners, water hoses and many other applications. In the oil and gas industry flexible pipes are used to extract oil and gas from the reservoirs and transport it up to the rigs. These corrugated pipes are called risers and need to be flexible so they can move around in the waves and ocean currents without being damaged. When extracting gas through these risers, a loud noise might be excited. This phenomenon is known as "singing" risers. The loud noise excited by the "singing" risers can make it hard to keep the rigs operational, and the vibrations can cause equipment fatigue, [1].

The "singing" riser phenomenon is a combination of different physical phenomena related to fluid dynamics and acoustics. A corrugated pipe is essentially a smooth pipe with a lot of small cavities. When gas flows through a corrugated pipe, small vortices are generated and travel across the cavities. These vortices might excite an acoustic frequency. The frequency excited depends on the size of the cavities, the flow velocity and the dimensions of the pipe. Even though there has been a number of publications regarding the phenomenon, the physical explanations are not yet clearly established. Previous work on the conundrum of "singing" risers has mostly been done by experimenting on small scale pipes with one or more cavities [2], and partially or fully corrugated pipes; [3], [4], [5] and [6] to mention some. In [7] the known physical mechanisms behind the whistling noise are described in detail.

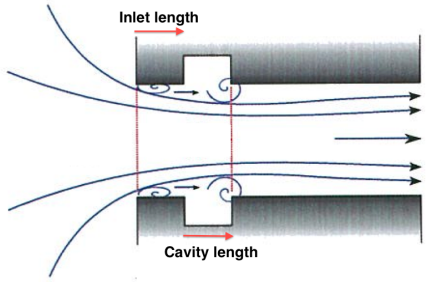

Figure 1.1: This figure is based on figure 1 in [2]: Vortices in a pipe with a single cavity.

This thesis will focus on the acoustic part of the "singing" risers phenomenon. It will be investigated by looking at a smooth pipe with a single cavity. Initially by simulations with different cavity lengths. The simulation software is not designed for acoustic calculations, so the results are validated using acoustic theory. Then experiments are conducted with different cavity and inlet lengths. Cancellation of the flow generated sound is also investigated by introducing an added cancellation frequency to the system.

Acknowledgements:
I would like to thank Ulf Kristiansen and Daniel Mazzoni. Ulf Kristiansen for excellent supervision and invaluable input through out the whole process. Daniel Mazzoni for Palabos code and other necessary assistance related to the use of the simulation software.

Chapter 2

Theory

2.1 Acoustic modes in a pipe

The length of a pipe will determine it's resonance frequencies. The resonance frequencies are recognized by a standing wave pattern in the pipe. For an open pipe end, the pressure is zero and the particle velocity is maximum. For a closed pipe end, the pressure is maximum and the particle velocity is zero. The standing pressure wave pattern formed in a pipe is therefore dependent on the boundary conditions at the ends of the pipe (See figure 2.1). Each resonance frequency is called an acoustic mode.

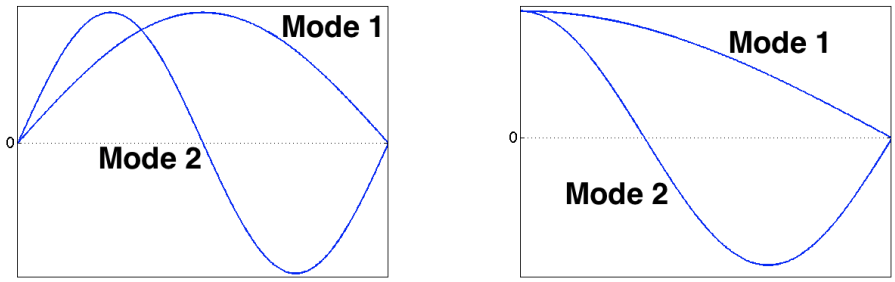

(a) Open - open: Mode 1 and 2

(b) closed - open: Mode 1 and 2

Figure 2.1: Standing pressure wave patterns

In this thesis two pipe configurations are used. A closed-open and an open-open pipe is used in the simulations, while in the experiments an open - open pipe is used. For a closed-open pipe the resonance frequencies f_n will occur when there are $\frac{(2n-1)}{4}$ wavelengths in the pipe. This makes the resonant wavelengths:

$$\lambda_n = \frac{4L}{2n-1} \tag{2.1.1}$$

where L is the length of the pipe and $n = 1, 2, 3....$

For an open - open pipe the resonance frequencies f_n will occur when there are $\frac{n}{2}$ wavelengths in the pipe. This makes the resonant wavelengths:

$$\lambda_n = \frac{2L}{n} \tag{2.1.2}$$

where L is the length of the pipe and $n = 1, 2, 3....$ The eigen frequencies are easily calculated by using

$$f_n = \frac{c}{\lambda_n} \tag{2.1.3}$$

For standing waves the pressure is leading the particle velocity with a phase of 90° , [8] [9].

2.1.1 Sound waves traveling in a pipe

The boundary conditions at the pipe ends will determine what happens to an acoustic wave when it reaches this boundary. For a closed and perfectly hard pipe end, the entire acoustic wave will be reflected from the boundary and travel back in the opposite direction. For an open end, the wave will both be transmitted through the open boundary and reflected back into the pipe due to an impedance difference. The result is that the standing wave in the pipe consists of a wave component A, traveling in the positive direction of the pipe, and a wave component B, traveling in the negative direction of the pipe. These two wave components superposed will make up the total standing wave pattern. The recorded standing wave in the simulation will look like the wave in figure 2.2(a), and the measured standing wave from the experiments will look like the wave in figure 2.2(b). A physically measured sound pressure will always be positive, so the negative part will appear positive, [8].

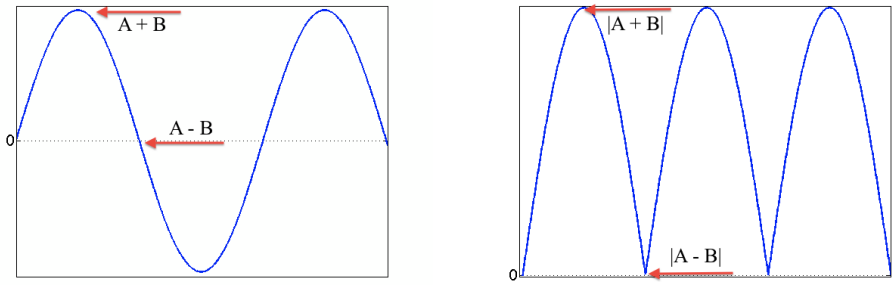

(a) A and B superposed as in the simulation.

(b) A and B superposed as measured.

Figure 2.2: The two wave components A and B superposed

2.2 Acoustic intensity and power

Intensity
Acoustic intensity is sound power per unit area. Instantaneous acoustic intensity for plane harmonic waves is given by:

$$\vec{I} = p\vec{u} \tag{2.2.1}$$

where p = density and u = particle velocity. The unit is $\frac{W}{m^2}$. The direction of the instantaneous intensity is the direction of the particle velocity. This expression is also valid for diverging waves far away from the source.

The time average of the instantaneous intensity is for plane harmonic waves is given by:

$$I = \frac{p^2}{2\rho_0 c} \tag{2.2.2}$$

where ρ_0 is the density of the medium and c is the speed of sound in the medium. The RMS intensity is given by

$$I_{\pm} = \frac{P_e^2}{\rho_0 c} \tag{2.2.3}$$

Power
Acoustic power is acoustic intensity multiplied with an area. For plane waves traveling in a pipe, the downstream power is the net intensity multiplied with the cross section of the pipe.

$$\prod_{downstream} = I_{net} \cdot \frac{\pi d^2}{4} \tag{2.2.4}$$

where d is the diameter of the pipe.

Upstream power can be approximated by looking at the pipe inlet as a source radiating sound spherically. Sound pressure is measured outside the pipe. It's assumed that there are no reflections outside the pipe, so the measured sound pressure level is from the pipe inlet only. With these assumptions, the upstream sound power outside a pipe is approximated by:

$$\prod_{upstream} = I_{outside} \cdot 4\pi r^2 \tag{2.2.5}$$

where r is the distance from the pipe inlet to the measuring point. This is the radius of a sphere with the pipe inlet as center. Additional details around the equations presented in this section can be found in [8].

2.3 End correction

The effective length of a smooth pipe depends on the pipe opening. If the pipe is unflanged the effective length L_{eff} is given by

$$L_{eff} = L + \frac{8r}{3\pi} \tag{2.3.1}$$

where L is the length and r is the radius of the pipe. If the pipe is flanged L_{eff} is given by

$$L_{eff} = L + 0.6r \tag{2.3.2}$$

Equation 2.3.1 and 2.3.2 are valid for wavelengths much larger than the pipe radius ($\lambda >> r$) [8]. For pipes with flares or cavities these results will be not be precise.

2.4 Dimensionless parameters

Several dimensionless parameters are widely used in fluid dynamics. The Reynolds number is related to the flow in fluid dynamics, [10]. The Strouhal number is related to oscillations in flow mechanics, [11]. Dimensionless power is introduced by [12] and is a normalization of power. Below are the formulas used in this thesis:

Reynolds number:

$$Re = \frac{vd}{w} \tag{2.4.1}$$

where v = flow velocity, d =pipe diameter, w = viscosity.

Strouhal number:

$$Sr = \frac{fL}{v} \tag{2.4.2}$$

where v = flow velocity, f =frequency, L = cavity length. The optimal Strouhal number, Sr_{opt}, is where the most power is generated in the system, [7].

Dimensionless power:

$$P_d = \frac{P_{source}}{\rho v S(\mid u' \mid)^2} \tag{2.4.3}$$

where P_{source} = source power, v = flow velocity, S = pipe cross section area, u = particle velocity.

2.5 The Lattice Boltzmann method

The lattice Boltzmann, LB, method is a cellular automata method. Cellular automata methods are described in [13]. In short, the Lattice Boltzmann method manages particle distributions on a lattice according to certain mathematical rules. Through time the particle distributions move around and collide. When distributions collide, collision rules are applied. The most common collision operator is

BGK. This is the operator used in the simulations in this thesis. The particle distributions on the lattice makes up the total fluid. The behavior is consistent with the Navier-Stokes equation.

In short the Lattice Boltzmann method consists of 4 steps:
The following is taken from page 26 of [13]:

" • Macroscopic quantities: From the current distribution of particles, calculate the macroscopic quantities.
• Equilibrium: Calculate the equilibrium distribution for each node from the nodes macroscopic variables.
• Collision: Calculate the post collision distribution of particles for all fluid nodes.
• Streaming: Move particles one step in the direction of their velocity."

2.6 Flow pipes and acoustics

When a liquid or a gas is flowing through a pipe, the flow can generally be either laminar or turbulent. A laminar flow occurs when the Reynolds number is less than approximately 2040. The fluid layers are in this case parallel and does not disturb each other, [14]. When the Reynolds number exceeds 2040 a turbulent flows starts to appear. For Reynolds numbers above 3000, flows are turbulent. A turbulent flow is characterized by the mixing of fluid layers, rapid pressure and velocity changes and is generally an unstable, [15].

In this thesis both simulations and experiments yield a high Reynolds numbers. The flows are therefore turbulent.

Simulation:

$$Re = \frac{10\frac{m}{s} \cdot 0.01m}{0.000015\frac{m^2}{s}} = 6667$$

Experiments:

$$Re = \frac{15.5\frac{m}{s} \cdot 0.043m}{0.000015\frac{m^2}{s}} = 44433$$

2.6.1 Vortices in flow pipes and whistling sounds

The physics behind whistling sounds in flow pipes are not clearly established. The most common theory is that vortices are generated by the cavity, and that this is what causes the flow generated whistling sound. In contrast, there is a theory stating that the cavity vortices are results of vortices generated at the inlet, and that without these inlet vortices no sound will be generated. Gas flowing through a pipe is picked up by the pipe inlet. When a flow is initiated the gas, in this case air, is drawn into the inlet. The flow is at this point unstable and inlet vortices are created because of the inlet edge. This coincides with [3] where a corrugated pipe section at the end of a smooth pipe not generated sound, while the same corrugated section at the beginning of the same pipe generated sound effectively. Applying the latter theory to these results leads to the explanation that the inlet vortices fade over distance. At the end of the pipe, the inlet vortices are either gone or not strong enough to be amplified by the corrugations. In [16] it's found that a round inlet edge will reduce the cavity flow substantially in Palabos simulations. It's also found experimentally that a rounded inlet edge will stop whistling sounds from being generated.

2.6.2 Hydrodynamic modes

The velocity of a vortex across a cavity is by [7] said to be $v_{vortex} = Sr \cdot v_{fluid}$. The period for a vortex to cross a cavity is then $t = \frac{Sr \cdot v_{fluid}}{lcav}$, making the frequency:

$$f = \frac{lcav}{Sr \cdot v_{fluid}} \tag{2.6.1}$$

By doing some simple algebraic manipulation, it's seen that this is the same equation as for the Strouhal number in section 4.2.3 (Equation 2.4.2). This frequency, at which vortices travel across the cavity, is called a hydrodynamic frequency. The situation when there is one vortex in the cavity at the time is called hydrodynamic mode 1. When there are two vortices in the cavity at the same time, it's called hydrodynamic mode 2. The speed of which a vortex travels across the cavity for hydrodynamic mode 2 is twice the speed of hydrodynamic mode 1. The likelihood for a whistling sound is high when a hydrodynamic mode frequency for the cavity coincides with an acoustic mode for the pipe, [5] [7].

2.6.3 Cancellation of flow generated frequency peaks with added sound.

Cancellation of whistling sound with the use of added sound is in theory possible by using the original signal with opposite phase. However, for this to work for an entire pipe system, the two signals must be 180° out of phase everywhere. This is not possible without an unlimited number of sound sources placed everywhere in the system. In order to cancel a flow generated frequency peak, the cancellation frequency must cancel the phenomena casing the sound in the first place. Previous research on cancellation includes [2], where an equivalent experimental setup as in this thesis was used. Here, an added frequency of 3086Hz dampened a 462Hz flow generated frequency peak from 108dB to 76dB. In [17] flow generated frequency peaks were strongly affected by a cancellation frequency of 10Hz. The peaks were either dampened or shifted to another modal order.

Chapter 3

Simulation and experiments

3.1 Simulations

In this section the simulations will be presented. This includes a presentation of the simulation software, the simulated situations and the data extraction. The motivation behind the simulations is to get a better understanding if Palabos is a viable software for simulating acoustics in a flow pipe. Also Palabos provides a visual understanding of the physical phenomena causing the whistling sound. This will be connected with the acoustic behavior of the system.

3.1.1 About the simulation and software

The simulation software used is Palabos, [18]. Palabos is an open source Lattice Boltzmann solver written in C++. The software can be used to describe and solve problems in fluid dynamics. For this thesis Palabos will be used to simulate a flow through a pipe in 2D with a single cavity. The code is written by Daniel Mazzoni [19], originally based on the showcase example "cylinder 2D" included in the Palabos package. As Palabos not is made for solving acoustic problems, the results will have to be analyzed with that in mind.

The base dimensions of the simulated pipe is described in figure 3.1. For the different simulation situations the only variable parameter was the cavity length (lcav). The system's total length was the same for all simulations, so the pipe

section downstream of the cavity was changed accordingly. The simulations were run on windows computers.

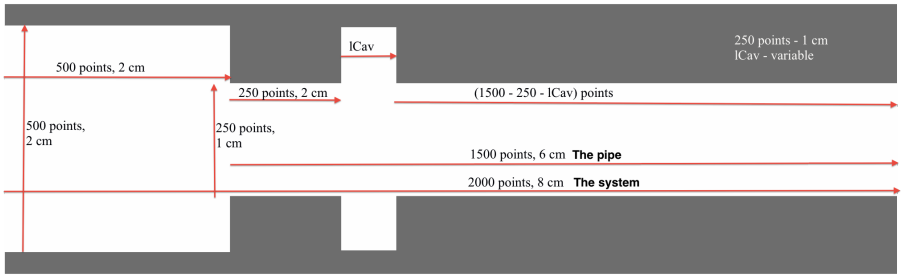

Figure 3.1: Simulated pipe.

Left of the inlet, there is defined an initial turbulent flow. On the right side there is an outlet flow condition. The other boundaries in the system were set as bounce back boundaries. Data was exported from 50 equally spaced locations along the center line of the pipe. Density and velocity data was stored along with images of the simulations. These images visualize the velocity of the fluid. Blue represents a low velocity and red represents a high velocity (See figure 4.12(e)). The parameters used in the simulations are the same as used by Daniel Mazzoni in [19], except for the mesh grid resolution. In this thesis *"system"* refers to the whole simulation domain. The *"pipe"* refers to the 1500 rightmost lattice points of the simulation domain, which is the pipe without the initial space.

Simulation Parameters:

- Domain size: 8cm x 2cm
- Mesh grid: 2000 x 500
- Length of the pipe: 6cm
- Length of the system: 8cm

- Inside diameter of the pipe: 1 cm
- Inside diameter of the system: 1cm / 2cm
- Length of the cavity: 0cm, 0.25cm, 0.33cm, 0.5cm and 0.67cm
- Height of the cavity: 0.5cm
- Dynamic viscosity of the fluid: $w = 0.000015 \frac{m^2}{s}$ (air)
- Velocity of the fluid at the center of the pipe: $v_0 = 10 \frac{m}{s}$
- Reynolds number based on these parameters: $Re = \frac{V_0 \cdot diameter}{w} = 6667$
- Reynolds number used in the simulation: $Re = 5800$

The Reynolds number used is lower than the Reynolds number which the parameters suggest. The reason is to get a stabile simulation. As the Reynolds number is describing the flow of the fluid, the theory is that it's of less acoustic importance. This will be discussed in section 5.1.1. Five different cavity lengths were simulated as indicated by the simulation parameters. Detailed unit convention calculations can be found in appendix A.1. From this it can be noted that for $lcav = 0.5cm$, the characteristic frequency, $f_0 = \frac{l_0}{v_0} = \frac{l_0/2}{v_0/2} = \frac{lcav}{vortexvelocity}$. This is valid if the Strouhal number is assumed to be 0.5 making the vortex velocity half of the flow velocity.

The simulation data will be interpreted with a sampling frequency of 100,000Hz. This is calculated in appendix A.1. Only frequencies below 40kHz will be discussed in this thesis as these are frequencies well above the audible limit. By using this sampling frequency only a small portion of the total frequency spectrum is studied (See figure A.3). There are uncertainties around unit conversion in Palabos. So the sampling frequency might not be correct. This is discussed further in section 5.1.2.

3.1.2 Theoretic acoustic modes for the simulations

The simulations are really two parallel situations:

- *The system:* A 8cm closed - open pipe with a cavity and an inlet area with increased diameter.

- *The pipe:* A 6cm open - open pipe with a cavity.

The theoretic acoustic modes for smooth pipes, with the same lengths and boundary conditions as used in the simulation, are shown in table 3.1.1.

Table 3.1.1: Theoretic eigenfrequencies for smooth pipes.

Pipe length	**8cm closed - open [Hz]**	**Pipe length**	**6cm open - open [Hz]**
$\frac{\lambda}{4}$	1063	$\frac{\lambda}{2}$	2833
$\frac{3\lambda}{4}$	3188	λ	5667
$\frac{5\lambda}{4}$	5313	$\frac{3\lambda}{2}$	8500
$\frac{7\lambda}{4}$	7438	2λ	11333
$\frac{9\lambda}{4}$	9563	$\frac{5\lambda}{2}$	14167
$\frac{11\lambda}{4}$	11688	3λ	17000
$\frac{13\lambda}{4}$	13813	$\frac{7\lambda}{2}$	198333
$\frac{15\lambda}{4}$	15938	4λ	22667
$\frac{17\lambda}{4}$	18063	$\frac{9\lambda}{2}$	25500
$\frac{19\lambda}{4}$	20188	5λ	28333
$\frac{21\lambda}{4}$	22313	$\frac{11\lambda}{2}$	311067
$\frac{23\lambda}{4}$	24438	6λ	34000
$\frac{25\lambda}{4}$	26563	$\frac{13\lambda}{2}$	36833

3.2 Experiments

In this section the physical experiments will be presented. This includes a presentation of the experimental setup and approach. The motivation behind the measurements is simply to study the generation, acoustic properties and possible cancellation of whistling sounds for this pipe geometry.

3.2.1 About the experimental setup

A similar experimental setup has previously been used by Mazzoni and Kristiansen [2] and Kristiansen and Wiik [3]. It consists of a metal pipe connected to a wooden box. The box acts as a flange on the outlet of the pipe and is large enough to make it an open pipe boundary. A 10 inch loudspeaker transducer is mounted on the side of the box facing inward making it a substantial part of the box wall. (See figure 3.2(c).) A vacuum cleaner is attached to the opposite side of the box and draws air through the pipe and the box. On the opposite end of the pipe, at the pipe inlet, there is attached an adjustable cavity end piece. (See figure 3.2(b).) This adjustable cavity can be set to lengths between $0mm$ and $21mm$. The total pipe length is extended by the cavity length as the cavity is increased. The pipe diameter is $43mm$ and the length with no cavity is $66cm$. The distance between the inlet and the cavity, the inlet length, is $1cm$ by default. By adding additional end pieces, the inlet length can be extended by $2mm$, $10mm$, $15mm$ and $20mm$, making the total inlet lengths $10mm$, $12mm$, $20mm$, $25mm$ or $30mm$.

Measurements were conducted with a probe attached to a microphone. This probe is a frequency dependent $67.5cm$ long tube with $1mm$ diameter. The probe enables measurements inside the pipe without severely altering the flow conditions. The microphone is connected to a band pass filter in order to filter out all frequencies except a band of 20Hz around the whistling frequency. At the outlet of the pipe a velocimeter is measuring the flow velocity in m/s. For these experiments an air speed of 15.5 m/s was chosen because it's a low velocity which still is exciting loud whistling frequencies.

A calibrator with 94dB output at 1000Hz was used on the microphone with the standard end cap. During calibration the bandpass filter was set to 990Hz-1010 Hz. As mentioned, measurements were conducted with a probe attached to the microphone instead of the standard end cap. For each mode, a measurement outside the pipe was conducted both with the probe and the standard end cap, in order to determine what effect the probe had on the measurements. The levels measured was read from an analogue voltmeter set to RMS slow. See appendix B.1 for details on the experimental equipment.

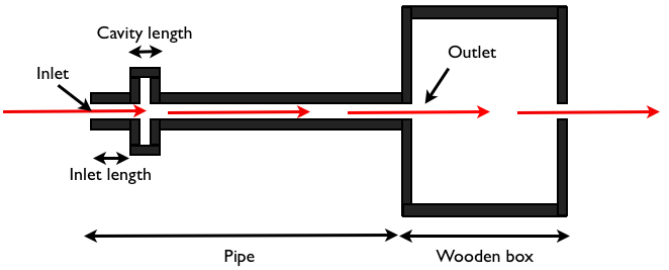

(a) Overview

(b) Pipe inlet with cavity and measuring probe,

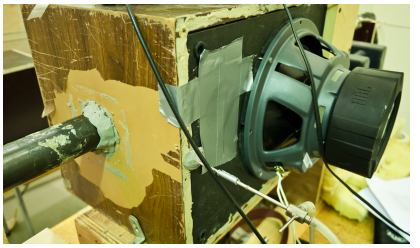

(c) Pipe outlet in a wooden box with an attached loudspeaker transducer.

Figure 3.2: The experimental setup.

Experimental data:

- Pipe length without cavity: $66cm$
- Pipe diameter: $43mm$
- Additional inlet lengths: $2mm$, $10mm$, $15mm$, and $20mm$,
- Cavity lengths: $1mm$ - $21mm$
- Cavity depth: $5mm$
- Flow velocity: 15.5 m/s

- Gas in pipe: Air
- Reynolds number in the experiments: $Re = 44433$

3.2.2 Theoretic acoustic modes for the experimental setup without a cavity

As the setup varies in pipe and cavity length there is a lot of possible eigenfrequencies. The length variations are small, so all the eigenfrequencies are very close. In table 3.2.1 the modes with the lowest and highest possible frequency are shown. The inlet end is unflanged and outlet end is flanged. End correction is applied accordingly. Calculations can be found in appendix B.2.

Table 3.2.1: Theoretic eigen frequencies for the experimental setup. (End correction applied)

Pipe length	**Inlet length**	**Cavity length**	**Eigen Frequencies**
65 cm	1.0 cm	0cm	Mode 1: 246 Hz
			Mode 2: 492 Hz
			Mode 3: 738 Hz
			Mode 4: 985 Hz
65 cm	3.0 cm	2.0 cm	Mode 1: 233 Hz
			Mode 2: 465 Hz
			Mode 3: 698 Hz
			Mode 4: 930 Hz

3.2.3 Measuring flow generated frequency peaks

The first measurement was done at $0mm$ cavity length. The cavity length was then increased by $1mm$ at the time. When an audible frequency peak was excited, 3 measurements were conducted: Maximum and minimum levels inside the pipe, and a measurement outside the pipe. As the modes in the pipe create a standing wave pattern, approximate locations for the maximum and minimum pressure are known from theory. Plane waves in the pipe were assumed, so the pressure in the pipe is assumed to be a function of the pipe length only. The anti nodes (maximum

pressure) are easy to measure due to the strong signal and large pressure top. The exact position of the nodes, (minimum pressure) can be hard to pinpoint exactly due to noise and the limited extent of the nodes in the pipe. (See figure 2.2(b).) For mode 1 at 230 Hz, the minimum pressure is at the pipe inlet and outlet. For this mode's minimum, end correction was applied as described in section 2.3.

For most cavity lengths one mode was dominant and therefore measured. In one case however, the dominant mode could be changed by for example blowing into the pipe (Increasing the air speed for a short period of time), or holding a hand close to the inlet (decreasing the air speed for a short period of time). In the case where this behavior was detected both modes were measured. Also, for short cavity lengths, no dominant modes were detected when increasing the cavity length from $0mm$ with the air flow running. When restarting the air flow however, some cavity lengths that did not excite a whistling sound previously, started exciting sound effectively. For these cavity lengths the case with a whistling sound is included in the results.

3.2.4 Flow generated frequency peaks cancelled with added sound

The loudspeaker mounted in the wooden box was used for cancellation. With a flow generated frequency peak excited, a slow frequency sweep was added in search of cancellation frequencies. When the flow generated peak was cancelled or changed by the added frequency, sound pressure levels were measured. Measurements were done on axis, $15cm$ from the pipe inlet. This experiment was done for mode 1, 2 and 3. Mode 1 was exited by a $14mm$ cavity and a $20mm$ inlet. Mode 2 was excited by a $15mm$ cavity and $10mm$, $12mm$, $25mm$ and $30mm$ inlet lengths. Mode 3 was excited by a $8mm$ cavity and a $20mm$ inlet.

Chapter 4

Results

In this chapter the results from the simulations and the experimental measurements are presented.

4.1 Simulation

From the Palabos simulations, frequencies below 40kHz will be studied. The first results presented are the frequency spectra and the pressure distributions in the system for the frequency peaks. Images of the simulations are provided along with a plot of the phase difference between pressure and particle velocity for the fundamental frequency. Then the magnitude of the 4 most important peaks are shown for all cavity lengths. Lastly, results regarding the instantaneous intensity at the downstream cavity wall, and the generation of inlet vortices are presented. "$lcav$" is short for cavity length.

4.1.1 Simulations with different cavity lengths

The frequency spectra in this section are the sum of all the 50 frequency spectra measured for the specific cavity length. The pressure curves are the pressure magnitude of the frequency in question plotted versus measuring points (length of the system). The vertical line plotted between measuring point 12 and 13 marks the inlet of the pipe.

The most dominant reoccurring peaks are named as follows:

- 1500-1800Hz: The 1st main peak.
- 33600Hz: The 2nd main peak.
- 37000 - 37800Hz: The 3rd peak.
- 17000 - 17700Hz: The 4th peak.

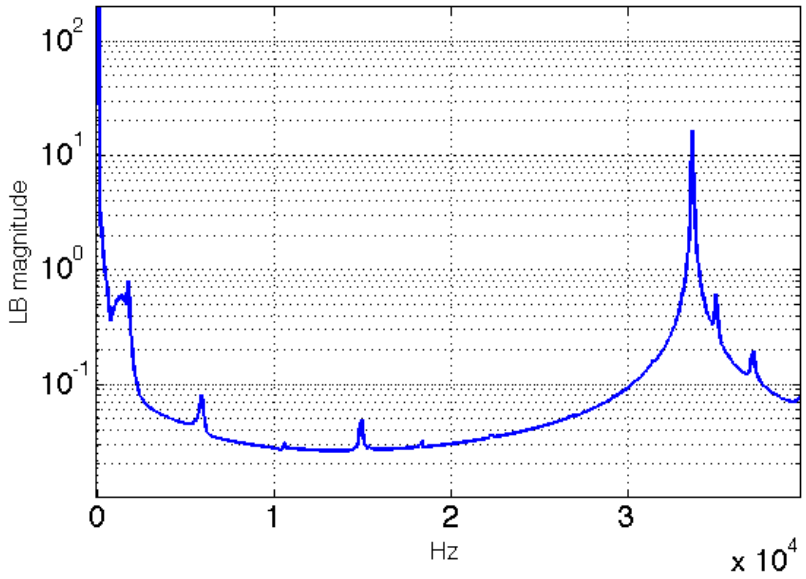

Figure 4.1: Frequency spectrum for $lcav = 0cm$

Comments: $lcav = 0cm$
The only peak below 33600Hz which appears to have acoustic relevance is the 1st main peak at 1699Hz. This peak is not dominant for this situation. The pressure distribution is a quarter of a wavelength in the system. The 2nd main peak at 33599Hz does not look like an acoustic wave. The 3rd peak at 37046Hz has $\frac{17}{4}$ wavelengths in the system.

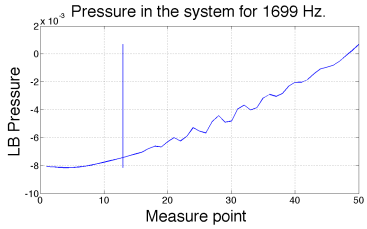

(a) 1699 Hz

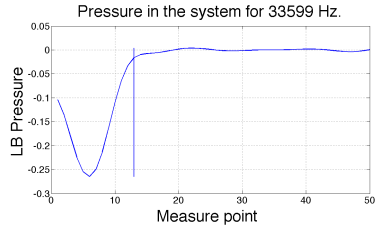

(b) 33599 Hz

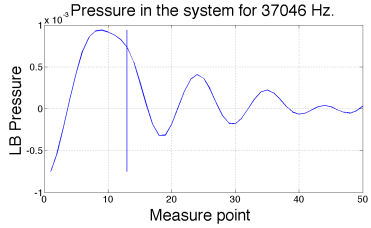

(c) 37046 Hz

Figure 4.2: Peaks with possible acoustic relevance for the $lcav = 0cm$ case.

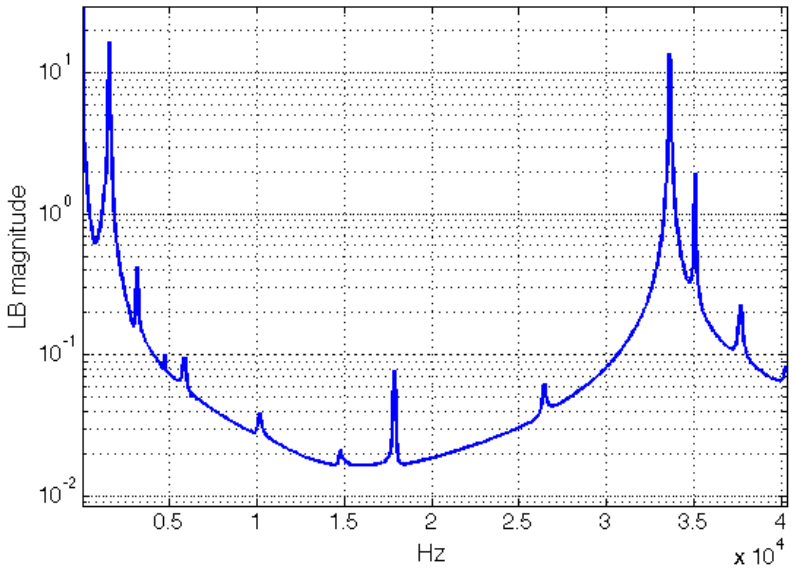

Figure 4.3: Frequency spectrum for $lcav = 0.25cm$

Comments: $lcav = 0.25cm$
For this situation there were more peaks than for the latter case. At 1554Hz the 1st main peak consist of a quarter of a wavelength in the system. The 2nd main peak at 33599Hz does now appear to coincide with acoustic theory with $\frac{5}{2}$ wavelengths in the pipe. The pressure curve of the 5875Hz peak has a clear acoustic appearance with $\frac{3}{4}$ wavelength in the system. The acoustic pressure curve for the 4th peak at 17868Hz, is the smoothest of the curves. The 3rd peak, now increased to 37677Hz, has $\frac{15}{4}$ wavelengths in the system. This is unexpected when comparing with the latter simulation. A frequency increase should result in more wavelengths in the system. In this case however, the number of wavelengths in the system has been reduced.

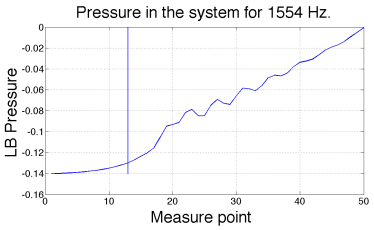

(a) 1554 Hz

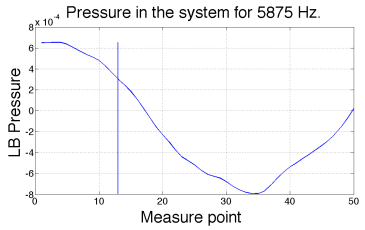

(b) 5875 Hz

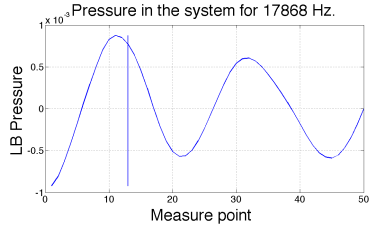

(c) 17868 Hz

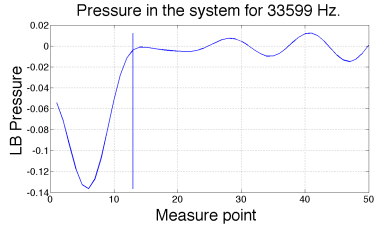

(d) 33599 Hz

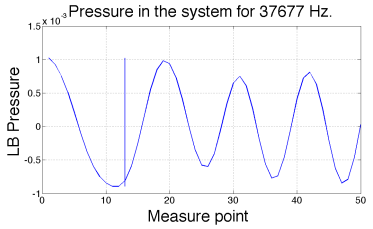

(e) 37677 Hz

Figure 4.4: Peaks with possible acoustic relevance for the $lcav = 0.25cm$ case.

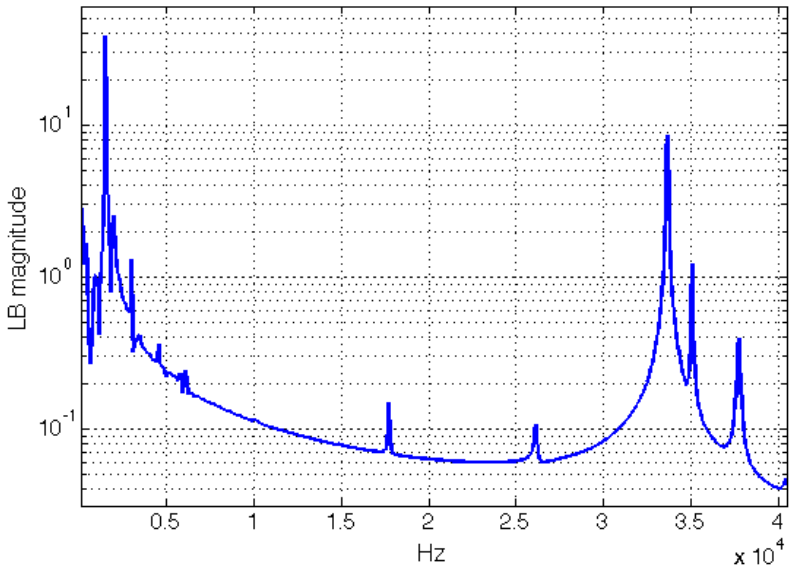

Figure 4.5: Frequency spectrum for $lcav = 0.33cm$.

Comments: $lcav = 0.33cm$
The 1st main peak, now at 1505Hz, does not appear to be acoustically relevant based on the pressure curve. The 1942Hz peak's pressure curve is a quarter of a wavelength in the system. The pressure curve for the 2nd main peak at 33647Hz is not zero at the pipe inlet, and thus it does not look exactly like an acoustic wave. The 3rd peak is at 37726Hz. The frequency is marginally higher than for the latter simulation, but there are only $\frac{13}{4}$ wavelengths in the system, which should have resulted in a lower frequency.

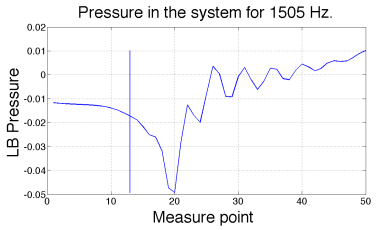

(a) 1505 Hz

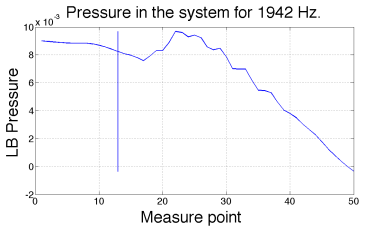

(b) 1942 Hz

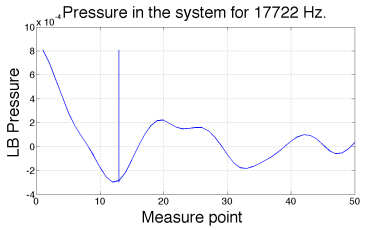

(c) 17722 Hz

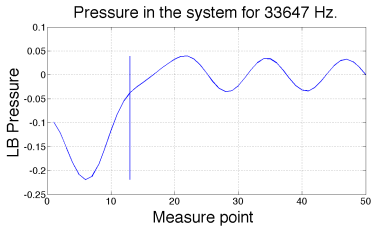

(d) 33647 Hz

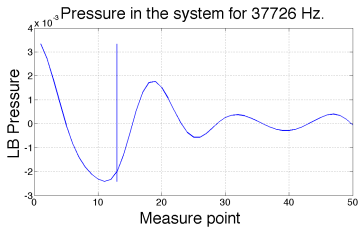

(e) 37726 Hz

Figure 4.6: Peaks with possible acoustic relevance for the $lcav = 0.33cm$ case.

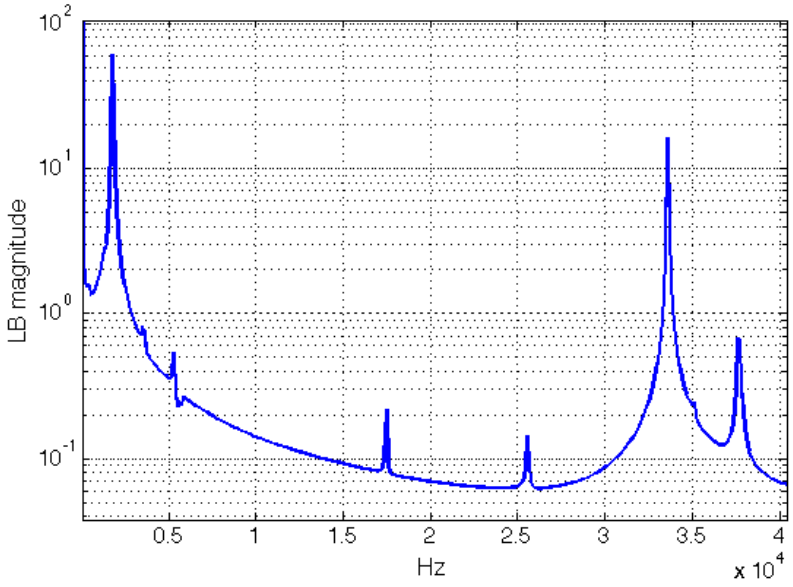

Figure 4.7: Frequency spectrum for $lcav = 0.5cm$

Comments: $lcav = 0.5cm$
Both the 1st and the 2nd main peak have acoustic pressure distributions. The 1st main peak is a quarter of a wavelength in the system, while the 2nd main peak has $\frac{5}{2}$ wavelengths in the pipe. This was also the case for the $lcav = 0.25cm$ situation. The pressure curves for the peak at 5341Hz and the 4th peak at 17479Hz has $\frac{3}{4}$ and $\frac{9}{4}$ wavelengths in the system. These two peaks have the same appearance as in the $lcav = 0.25cm$ case, but the frequencies have decreased. The 3rd peak at 37637Hz is now $\frac{15}{4}$ wavelengths in the system. The frequency is very close to the $lcav = 0.25cm$ case, and the number of wavelengths in the pipe is the same.

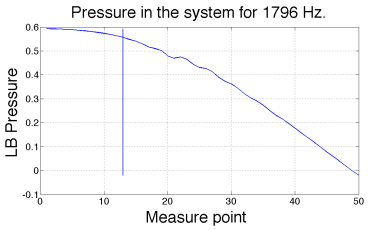

(a) 1796 Hz

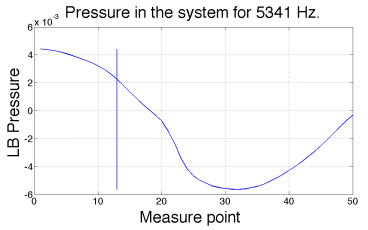

(b) 5341 Hz

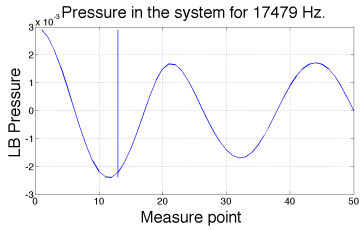

(c) 17479 Hz

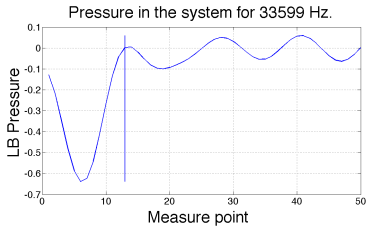

(d) 33599 Hz

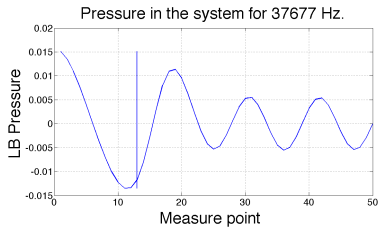

(e) 37677 Hz

Figure 4.8: Peaks with possible acoustic relevance for the $lcav = 0.5cm$ case.

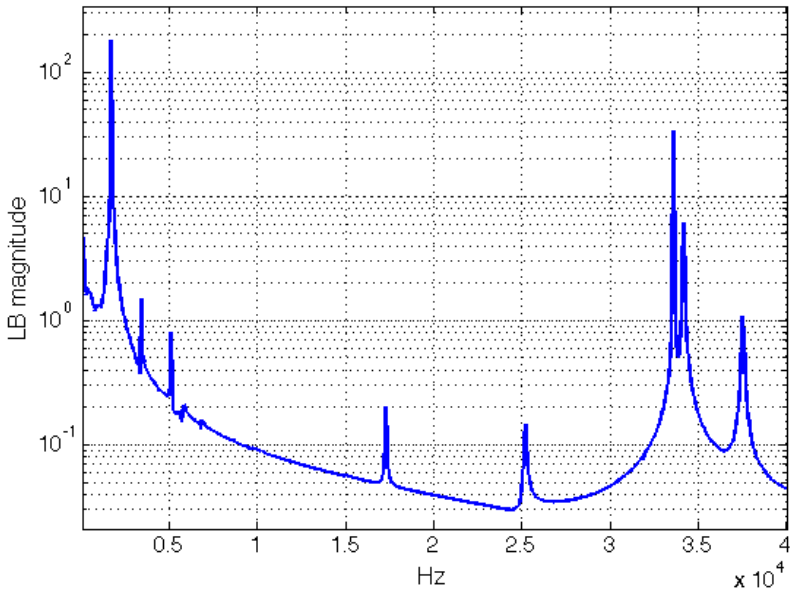

Figure 4.9: Frequency spectrum for $lcav = 0.67cm$

Comments: $lcav = 0.67cm$
As for 0.25cm and 0.5cm cavity lengths the two main peaks looks like acoustic modes. There is a quarter of a wavelength in the system for the 1st main peak at 1699Hz, and $\frac{5}{2}$ wavelengths in the pipe for the 2nd main peak at 33599Hz. The pressure curve for the 4th peak at 17285Hz is like in the latter case; a smooth curve of $\frac{9}{4}$ wavelengths in the system. The frequency is now lower than the previous case for the same amount of wavelengths in the system. The 3rd peak at 37532Hz is the result of a pressure wave with $\frac{17}{4}$ wavelengths in the system. This frequency is marginally lower, but consists of more wavelengths in the system than the three previous cases.

Comments: Phase difference
The linearized phase difference between pressure and particle velocity in the pipe downstream of the cavity is declining from 94° to 78° (Red line in figure 4.11). The theoretical phase difference for standing waves is 90° (See section 2.1). The phase difference in the rest of the system is not plotted because of undefinable results.

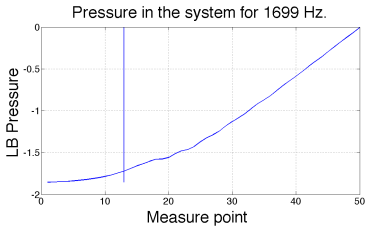

(a) 1699 Hz

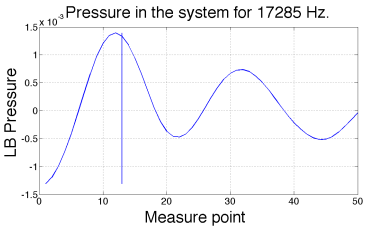

(b) 17285 Hz

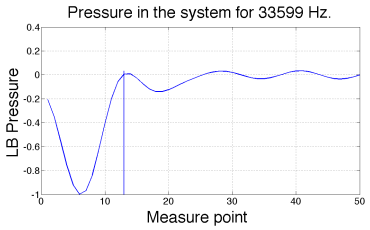

(c) 33599 Hz

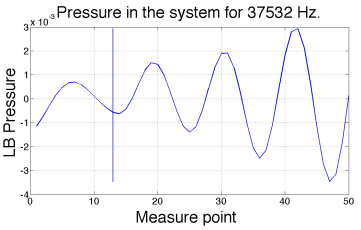

(d) 37532 Hz

Figure 4.10: Peaks with possible acoustic relevance for the $lcav = 0.67cm$ case.

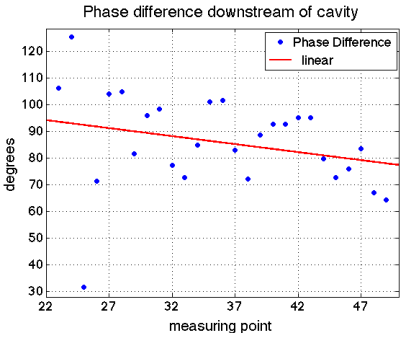

Figure 4.11: Phase difference between pressure and particle velocity in the pipe, downstream from the cavity.

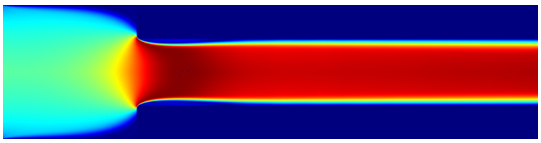

(a) Cavity = 0 cm

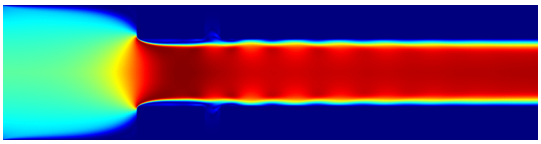

(b) Cavity = 0.25 cm

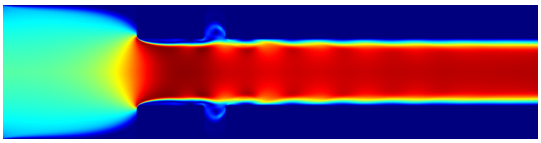

(c) Cavity = 0.33 cm

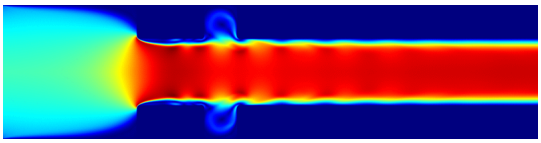

(d) Cavity = 0.5 cm

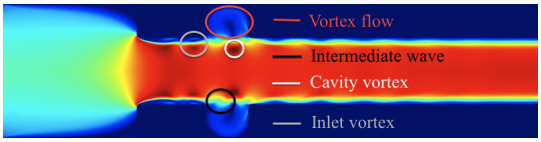

(e) Cavity = 0.67 cm

Figure 4.12: The simulation situations.

Comments: The simulation situations
In figure 4.12 where the different simulation situations are shown, the trend is that a longer cavity length equals a larger cavity flow, intermediate waves and cavity vortices. The differences in velocities in the systems can be seen by studying the colors in the figure. Figure 4.12(d) gives a visual explanation of the different phenomena in the pipe.

4.1.2 Magnitude of the reoccurring peaks

The maximum magnitude for the four labeled peaks are plotted versus cavity length. The peak magnitudes plotted are calculated with $\sqrt{f_{p-1}^2 + f_p^2 + f_{p+1}^2}$, where f_p is the peak frequency.

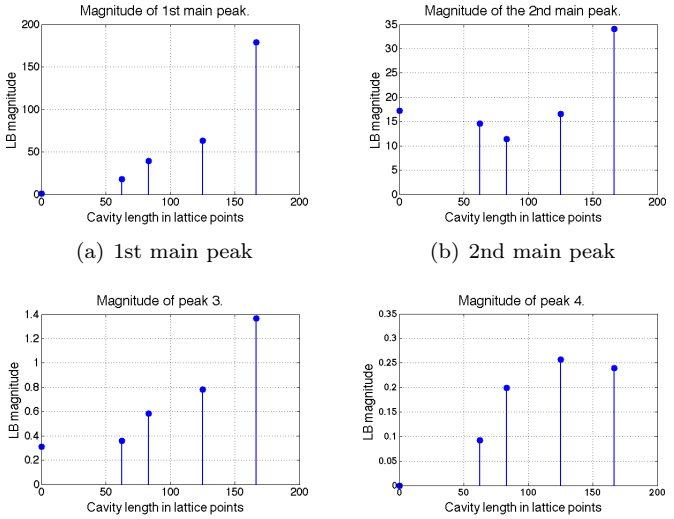

(a) 1st main peak (b) 2nd main peak

(c) 3rd peak (d) 4th peak

Figure 4.13: Magnitude of the reoccurring peaks versus cavity length.

Comments: Magnitude of reoccurring peaks
The magnitude of the 1st main peak shows that increased cavity length leads to increased amplitude. For the 2nd main peak the longest cavity length will also excite the maximum peak magnitude, but the second highest magnitude is for no cavity at all. The 3rd peak does also have a magnitude which increases when the cavity length is increased. The 4th peak is not present when there is no cavity. The magnitude increases with the cavity length, until $lcav = 0.67cm$ where it's slightly reduced from $lcav = 0.5cm$.

4.1.3 Cavity intensity

By multiplying the measured particle velocity and pressure at the downstream cavity wall, the instantaneous intensity at this point is found (See theory in section 2.2.) By comparing the instantaneous intensity and images from the simulation, the generation of intensity can be investigated. The maximum instantaneous intensity throughout the pipe is plotted to see where in the system the maximum occurs. Except for measuring point 19-22, which is the cavity, the data is smoothed using a 3-point average. Smoothing was not used on the cavity data as the spatial resolution is too low. This is done to better illustrate the cavity effect. With a higher spatial resolution this would not be necessary. The $lcav = 0.5cm$ case is used for the instantaneous intensity analysis.

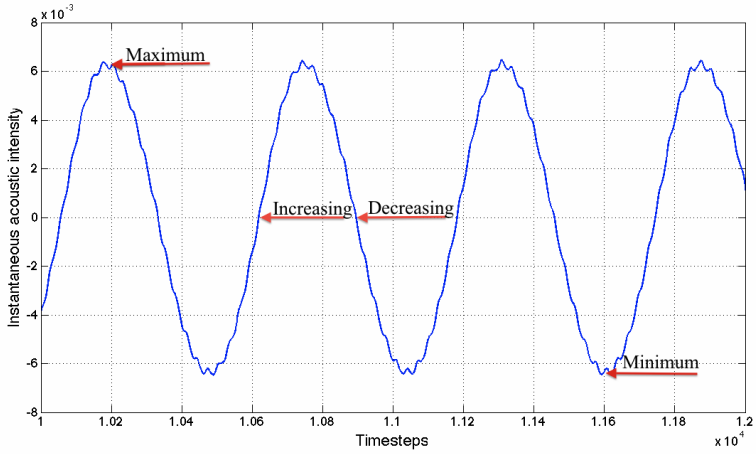

Figure 4.14: Instantaneous intensity at the downstream edge of the cavity.

Comments: Instantaneous intensity at the downstream cavity edge
Maximum instantaneous intensity is when a cavity vortex just has passed the cavity. At this time the intermediate wave is at the measuring position. The minimum instantaneous intensity is when a cavity vortex is about to hit the downstream cavity edge. In general, the maximum instantaneous intensity is increasing throughout the system, with a significant peak in the cavity where the intensity is at a maximum.

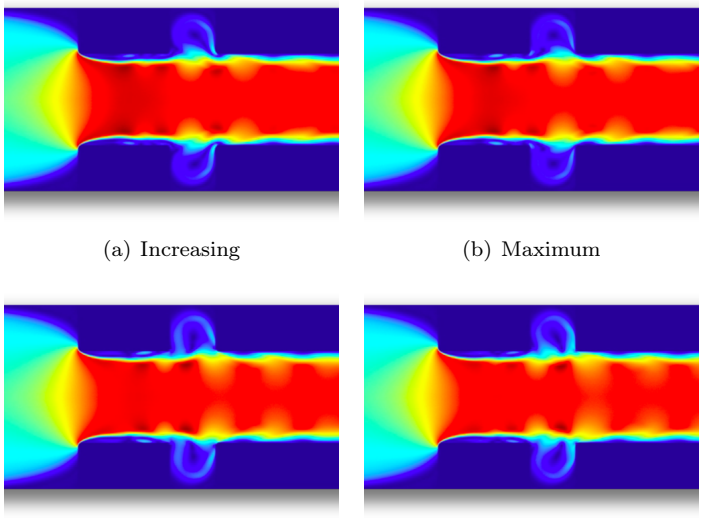

(a) Increasing (b) Maximum

(c) Decreasing (d) Minimum

Figure 4.15: Situation in the pipe for maximum, decreasing, minimum and increasing instantaneous intensity. $lcav = 0.5cm$.

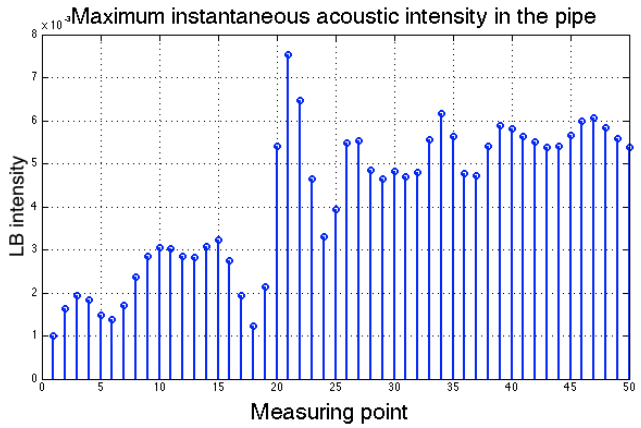

Figure 4.16: Maximum instantaneous intensity in the system. The data is smoothed except for in the cavity.

4.1.4 Inlet vortices

The generation of inlet vortices can be investigated by comparing images from the simulation with pressure and velocity data at the inlet.

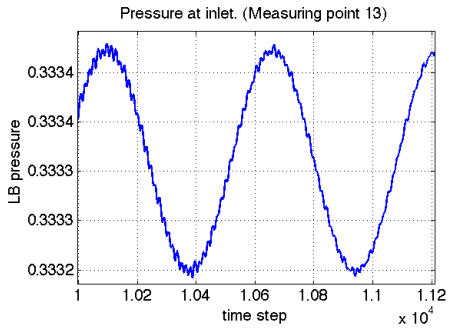

(a) Pressure at inlet

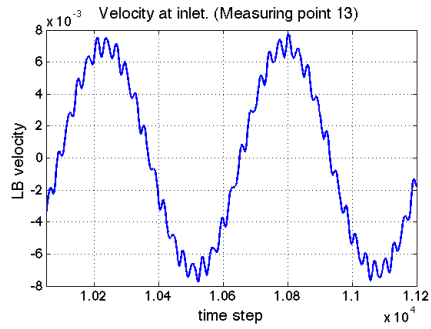

(b) Velocity at inlet (Fluctuating part)

Figure 4.17: Pressure and velocity at inlet. Time step = 10000 - 11200.

Comments: Generation of inlet vortices
The vortices near the inlet are hard to pinpoint exactly from the images in figure 4.18. The black circles are highlighting the location of an inlet vortex being generated. The white circles highlight a vortex entering the cavity. There is a pressure maximum at the inlet when an inlet vortex is half way down the inlet section of the pipe, and a cavity vortex has reached the downstream cavity edge. A pressure minimum occurs when a cavity vortex is half way down the cavity. At this point it appears to be two inlet vortices in the inlet section of the pipe. The velocity is at a maximum when an inlet vortex is entering the cavity, and at a minimum when a cavity vortex is about to hit the downstream cavity wall. Specific properties for the inlet vortices are hard to identify at the velocity minimum and maximum. From figure 4.17 is is observed that the pressure curve is leading the velocity curve at the inlet with close to 90°.

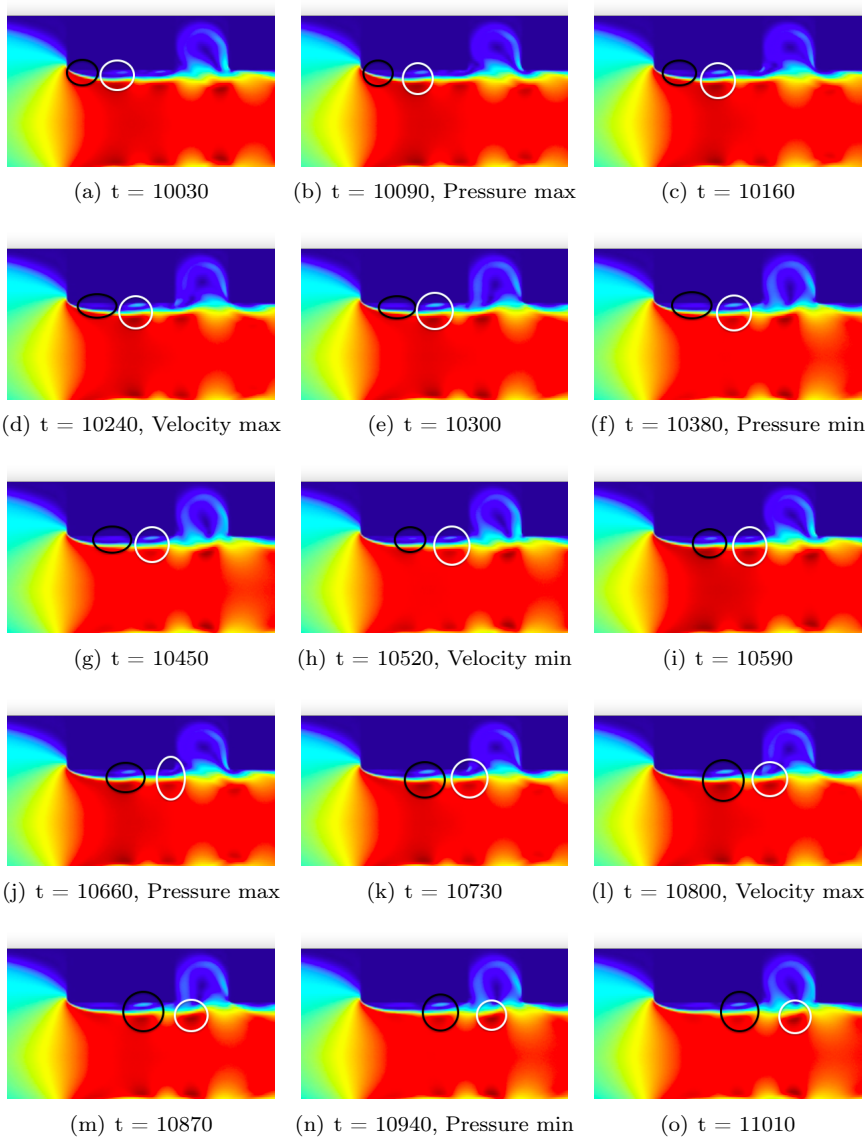

(a) t = 10030 (b) t = 10090, Pressure max (c) t = 10160

(d) t = 10240, Velocity max (e) t = 10300 (f) t = 10380, Pressure min

(g) t = 10450 (h) t = 10520, Velocity min (i) t = 10590

(j) t = 10660, Pressure max (k) t = 10730 (l) t = 10800, Velocity max

(m) t = 10870 (n) t = 10940, Pressure min (o) t = 11010

Figure 4.18: Situation at time step t. The black circle indicates the position of an inlet vortex being generated. The white circle indicates the position of an inlet vortex entering the cavity.

4.2 Experiments

The inlet length is $1cm$ by default. Measurements were conducted for $2mm$, $10mm$, $15mm$ and $20mm$ added inlet length. This makes the total inlet lengths: $10mm$, $12mm$, $20mm$, $25mm$ and $30mm$. The measured frequencies were in accordance with the theoretical frequencies in table 3.2.1, and can be found in appendix B.3.

4.2.1 Sound pressure level

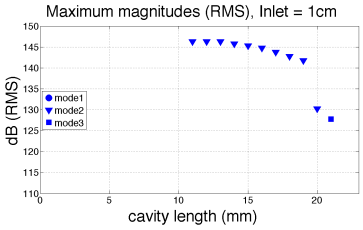

(a) Inlet length: 10mm

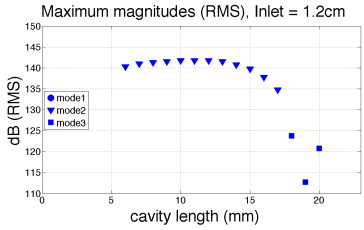

(b) Inlet length: 12mm

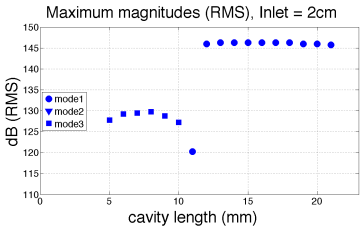

(c) Inlet length: 20mm

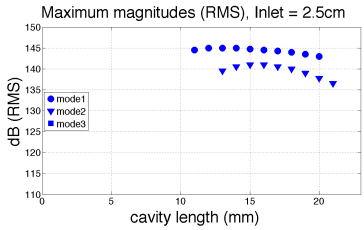

(d) Inlet length: 25mm

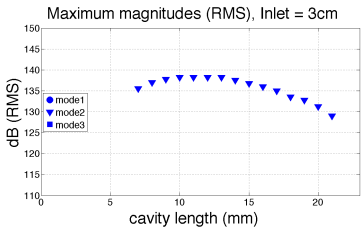

(e) Inlet length: 30mm

Figure 4.19: Maximum sound pressure level in the pipe (RMS).

Table 4.2.1: The generation of sound for short cavity lengths when restarting the airflow.

Inlet	**lcav**	**Mode**	**Frequency peak**	**Consistency**
10mm	8-9mm	2	When restarting flow	Fades quickly
10mm	10mm	2	When restarting flow	Fades after a while
10mm	11mm	2	When restarting flow	Does not fade
10mm	12mm	2	Self generated	Does not fade
–	–	–	–	–
12mm	6mm	2	When restarting flow	Does not fade
12mm	7mm	2	Self generated	Does not fade
–	–	–	–	–
20mm	5mm	2	Self generated	Does not fade
–	–	–	–	–
25mm	5-11mm	2	When restarting flow	Fades quickly
25mm	12mm	2	When restarting flow	Fades away
25mm	13mm	1 or 2	Self generated	Does not fade
–	–	–	–	–
30mm	6mm	2	When restarting flow	Fades quickly
30mm	7mm	2	Self generated	Does not fade

Comments: Maximum pressure antinodes
The maximum pressure was measured at antinodes in the pipe. For the two shortest inlets mode 2 was excited at most cavity lengths. Mode 3 appeared at longer cavity lengths. For an inlet of $20mm$ mode 3 was exited at cavity lengths up to $10mm$. From there mode 1 took over with a steady maximum level up to $lcav = 21mm$. With an inlet of $25mm$ mode 1 was basically unchanged from the latter situation. In addition to mode 1 it was possible to switch to mode 2, and back. This was done as described in section 3.2.3. For the $30mm$ inlet, mode 2 was excited for all sound generating cavity lengths, with a maximum level between $10mm$ and $13mm$.

Comments: Whistling for short cavity lengths
A descriptive overview of short cavity lengths and the duration of whistling sounds can be found in table 4.2.1. It shows that a short cavity results in either no sound at all, or a sound of short duration when the airflow is restarted. Longer cavity lengths result in a continuos sound.

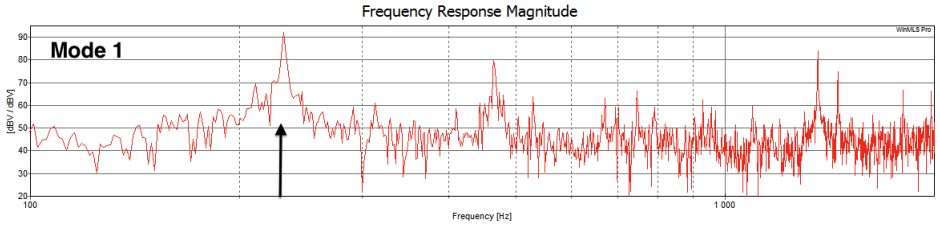

(a) Mode 1 excited

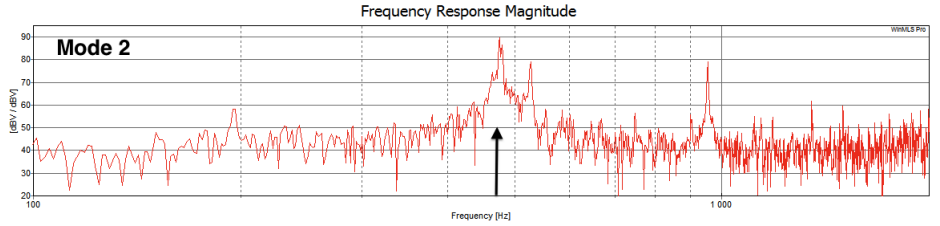

(b) Mode 2 excited

Figure 4.20: The frequency spectrum for mode 1 and 2 in the case where both modes were possible to excite for the same cavity and inlet length. Inlet length $= 25mm$, $lcav = 15mm$.

Comments: Frequency spectrum for mode 1 and 2
When mode 1 was the dominant whistling sound the harmonics excited were mode 2 and a peak slightly above 1000Hz. When mode 2 was dominant mode 4 was exited. See table 3.2.1 for a mode overview.

4.2.2 Power

The intensity was found by first finding the downstream A, and upstream B, wave components (See section 2.1). Then equation 2.2.3 was used to calculate the downstream and upstream intensity. Intensity plots can be found in appendix B.4. As plane waves in the pipe are assumed, the downstream power was found by using equation 2.2.4. An upstream power approximation was found by using equation 2.2.5. Measurements outside the pipe can be found in appendix B.4.

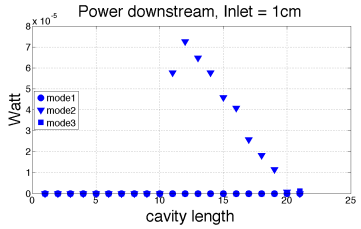

(a) Inlet length: 10mm

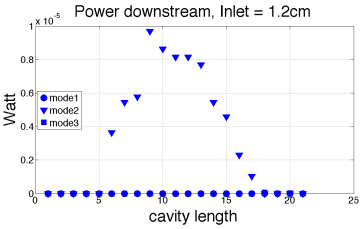

(b) Inlet length: 12mm

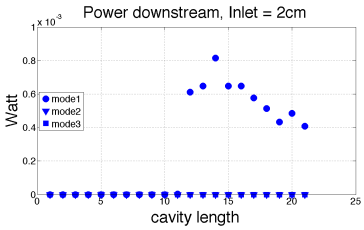

(c) Inlet length: 20mm

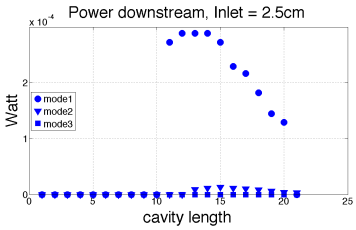

(d) Inlet length: 25mm

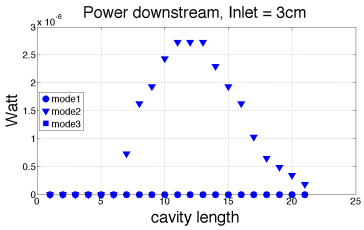

(e) Inlet length: 30mm

Figure 4.21: Downstream power (RMS).

Comments: Downstream power
The downstream power is for all inlet lengths generally largest for cavity lengths between $9mm$ - $14mm$. The modes which only are excited at low or high cavity lengths does not produce a lot of downstream power.

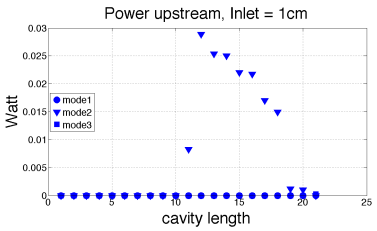

(a) Inlet length: 10mm

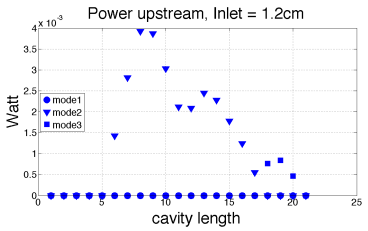

(b) Inlet length: 12mm

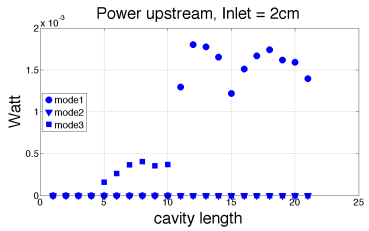

(c) Inlet length: 20mm

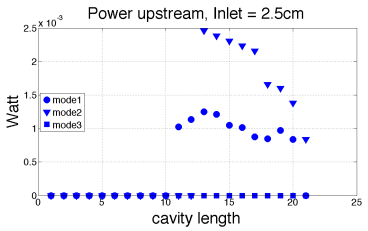

(d) Inlet length: 25mm

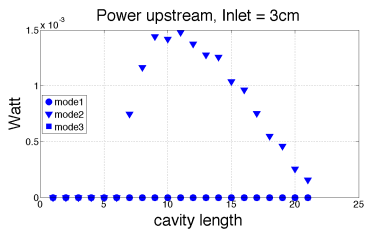

(e) Inlet length: 30mm

Figure 4.22: Upstream power approximation (RMS).

Comments: Upstream power
The upstream power is in all cases higher than the downstream power. For the $25mm$ inlet, mode 2 is generating more power than mode 1. This is opposite of the case for the downstream power. The maximum upstream power is generated for cavity lengths between $8mm$ - $18mm$. This is a wider range than for the downstream power.

4.2.3 Dimensionless Power

In this section dimensionless power is plotted versus Strouhal number. The power results are normalized as in decried in section 4.2.3. [12]

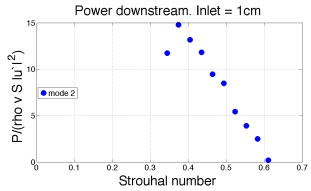

(a) Mode 2, Inlet length: 10mm

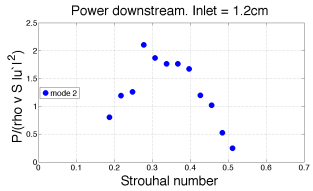

(b) Mode 2, Inlet length 12mm

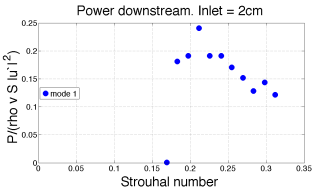

(c) Mode 1, Inlet length 20mm

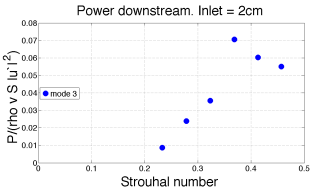

(d) Mode 3, Inlet length 20mm

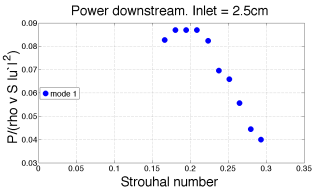

(e) Mode1 Inlet length 25mm

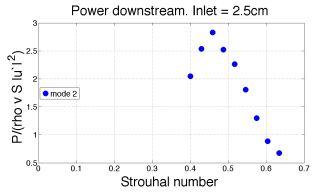

(f) Mode2, Inlet length 25mm

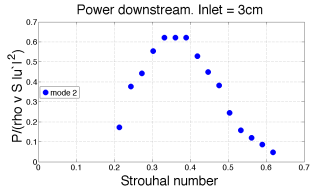

(g) Mode 2, Inlet length 30mm

Figure 4.23: Dimensionless downstream power versus Strouhal number.

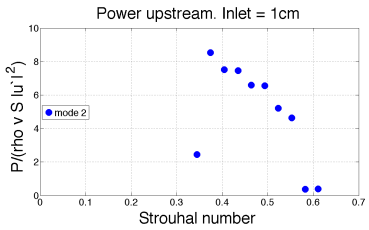

(a) Mode 2, Inlet length 10mm

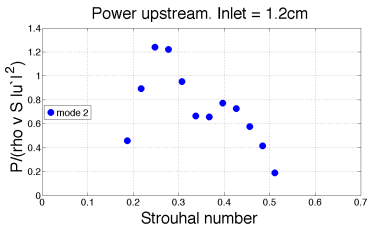

(b) Mode 2, Inlet length 12mm

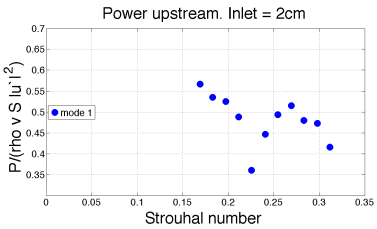

(c) Mode 1, Inlet length 10mm

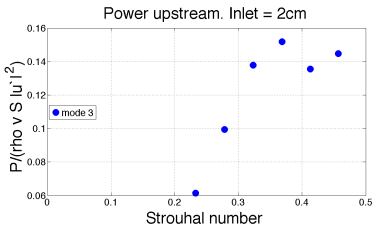

(d) Mode 3, Inlet length 20mm

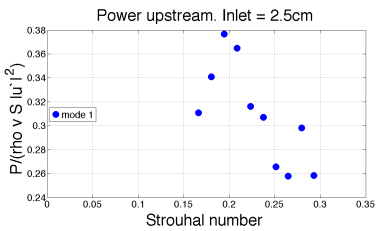

(e) Mode 1, Inlet length 25mm

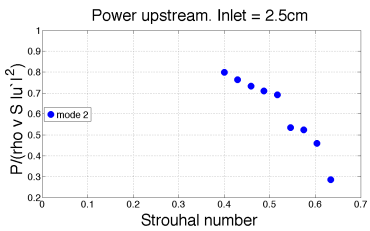

(f) Mode 2, Inlet length 25mm

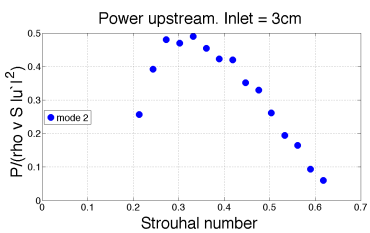

(g) Mode 2, Inlet length 30mm

Figure 4.24: Dimensionless upstream power versus Strouhal number.

Comments: Dimensionless power
The plots of downstream dimensionless power appears smooth with one peak. These peaks are at a Strouhal number in the 0.2 - 0.5 range. For the upstream dimensionless power the results are more rough. There can be one or two peaks, or simply a decline from a high power magnitude. Considering both the upstream and downstream dimensionless power, the power peaks for mode 1 are close to Strouhal number; $Sr_{opt} = 0.2$. For mode 2 and 3 the power peaks are mostly in the Strouhal number range; $Sr_{opt} = 0.3$ - 0.4.

4.2.4 Cancellation with added sound

In this section f_f and A_f is the flow generated frequency and amplitude. f_a and A_a is the added frequency and amplitude.

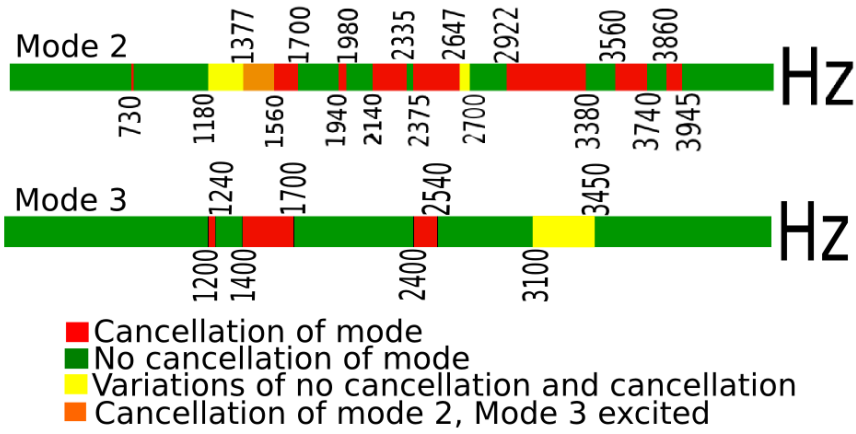

Figure 4.25: Flow generated acoutic mode 2 and 3: Response to an added sound of 50Hz - 4500Hz. Mode 2: $lcav = 15mm$, Inlet length $= 12mm$. Mode 3: $lcav = 8mm$, Inlet length $= 20mm$.

Table 4.2.2: Cancellation of mode 2: f_f = 480Hz, lcav = 15mm.

Inlet length	A_f	f_a **(Hz)**	A_a	**Change**
10mm	105dB	–	–	f_f not cancelled
12mm	100dB	1180 - 1200	93dB	Change to mode 2 and 3
12mm	100dB	1430	96.5dB	Changes to mode 3
12mm	100dB	1666	92.9dB	f_f cancelled
12mm	100dB	2140	89dB	f_f cancelled
12mm	100dB	2380-2442	85.5dB	f_f cancelled
12mm	100dB	2900-3005	84.5dB	f_f cancelled
12mm	100dB	3650	83.5dB	f_f cancelled
12mm	100dB	3840	90.5dB	f_f cancelled
25mm	101dB	–	–	f_f not cancelled
30mm	96dB	1130	93.5dB	f_f cancelled
30mm	96dB	1390	101dB	f_f cancelled
30mm	96dB	1600	101dB	f_f cancelled

Table 4.2.3: Cancellation of mode 3: f_f = 714Hz, lcav = 8mm.

Inlet length	A_f	f_a **(Hz)**	A_a	**Change**
20mm	96dB	1200	91dB	f_f cancelled
20mm	96dB	1420	97.5dB	f_f cancelled
20mm	96dB	1460	91dB	f_f cancelled
2a0mm	96dB	1525	89.5dB	f_f cancelled

Comments: Cancellation frequencies
In table 4.2.2 and 4.2.3 some of the cancellation frequencies and levels for mode 2 and 3 are shown. For a cavity length of $15mm$, mode 2 was excited for all inlet lengths except $20mm$. For $10mm$ and $25mm$ inlet lengths, no cancellation frequencies were found. For inlet lengths of $12mm$ and $30mm$, f_f could be cancelled for a number of f_a. Mode 3 was only excited as a dominant mode for the $20mm$ inlet. Mode 1, excited by a $10mm$ inlet and a $14mm$ cavity, was only cancelled for f_a = 1630Hz - 1650Hz. The amplitude of the cancellation frequencies were in general lower than the whistling frequency at the measuring position for all modes.

Chapter 5

Discussion

5.1 Simulation

In figure 4.12, images from the different simulation situations are shown. There are two different vortices in these simulations: Inlet vortices and cavity vortices. In addition there is a cavity flow of low velocity going counter clockwise around the cavity. It's starting at the downstream cavity edge and ending at the upstream cavity edge. At this point it's feeding down into the pipe flow. The inlet vortices are recognized by a light blue area close to the pipe wall, and a corresponding yellow and red area in the pipe flow. These vortices are generated by the initial unstable flow and the inlet edges. They are traveling downstream along the pipe wall. When the inlet vortices arrive at the upstream cavity edge they are amplified by the cavity flow, which is feeding fluid back into the pipe stream. These amplified vortices are called cavity vortices, as they travel in the cavity. A cavity vortex is recognized by a dark area in the red pipe flow. The larger blue and yellow area following a cavity vortex is an intermediate wave connecting the vortices. When cavity vortices hit the downstream cavity edge they are partially picked up by the cavity flow and partially continuing down the pipe stream where they fade away. This motion, which is consistent with hydrodynamic mode 1, repeats itself throughout the simulations. For the case with no cavity, the inlet vortices generated by the initial unstable flow are not amplified. The result is that the system not is excited, and the inlet vortices fade away.

The size of the flow in the cavity is clearly a result of the cavity size. A larger cavity will produce a larger flow as the flow uses more of the vertical space in the cavity.

A larger cavity flow will amplify the inlet vortices more than a small cavity flow. This effect is best seen in an animation, but a change in color, which represents a change in velocity, can be seen in the still pictures in figure 4.12 and 4.18.

5.1.1 Pressure analysis

In section 4.1.1 the added frequency spectra for all measuring points are plotted for each cavity length. To identify which peaks that have acoustic relevance, the pressure along the horizontal axis in the system are compared with theory of acoustic modes in pipes. Specifically pipes with boundary conditions closed - open and open - open, as described in section 2.1. By looking at the pressure in the system, the peaks with possible acoustic relevance are recognized. The pressure curves for the relevant peaks are plotted in section 5.1.1. In appendix A.2 pressure curves for peaks with questionable acoustic relevance are plotted. When analyzing the system pressure, it's important to note that the system does not have the properties of a perfect pipe. The cavity, the flow and the space before the pipe inlet will affect the results. Therefore, when analyzing the system pressure, an acoustic mode might not appear as smooth as if the cavity or space before the inlet not was present. In these simulations the effects of the initial space can not be avoided. The frequency responses show that different cavity lengths result in different frequency peaks. For the case without a cavity, the 2nd main peak is the only dominant peak. Below 33600Hz there are a lot of different peaks of low magnitude for the different situations including the 4th peak at 17000Hz - 17700Hz. Compared to the main peaks these peaks are small, but because they change when the cavity length is changed they are still of interest. Above the 2nd main peak there are two peaks. One at 35000Hz, which not is acoustic, and the 3rd peak at 37000Hz - 37700Hz.

The 1st main peak

In figure 4.17(a), a small part of the pressure time series is plotted for the $lcav = 0.5cm$ case. When comparing with exported images of the LB simulation, in figure 4.18, it's clear that one period of the longest wavelength is one cavity flow period. This is the frequency of the 1st main peak. This peak is dominant for all cavity lengths with a pressure distribution of a quarter wavelength in the system. The fact that this peak is negligible for the case without a cavity indicates that cavity effects are exciting this system mode. On the other hand, the 1505Hz peak for the $lcav = 0.33cm$ case has a different, non acoustic pressure distribution (See figure 4.6(a)). The pressure curve which is more consistent with a quarter of a wavelength is 1942Hz, but this curve is also rough. Unknown effects in the LB

fluid simulations could cause these rough curves. The theoretic frequency for a quarter wavelength in the system is 1062Hz. This is 50% - 60% lower than the simulated 1500Hz - 1800Hz. Still, the 1st main peak is certainly excited by the cavity, and a longer cavity equals a stronger peak (See figure 4.13(a)). The phase difference between pressure and particle velocity for this frequency is plottet in figure 4.11. Downstream of the cavity the phase difference is declining from 94° to 78° through the pipe. The decrease is probably the result of absorption by the gas viscosity. A phase difference of 90° is expected from an acoustic wave (section 2.1), so this result supports that the peak is acoustic.

The 2nd main peak

The shorter wavelength in figure 4.17(a) is the 2nd main peak. This peak is present for all simulations, with pressure curves in the pipe approximately the same for all cases. The curve for the $lcav = 0cm$ case is different by being more rough. Also, the boundary condition at the pipe inlet is not satisfied. The latter is also the case for $lcav = 0.33cm$. This could suggest that the peak is not acoustic, or it could be a result of effects caused by the cavity or inlet. For the other cavity lengths, the boundary conditions are satisfied and there are $\frac{5}{2}$ wavelengths in the pipe. The theoretic frequency for a smooth pipe would be 14167Hz, which is about 60% lower than the simulated frequencies. As this peak is present in all simulations, it's not excited by cavity effects. There is no trend towards increasing magnitude with increasing cavity length, or other evidence pointing towards an acoustic origin of this peak.

The 3rd peak

The 3rd peak's pressure distribution is for all cases consistent with that of an acoustic wave. Still, the variation between the frequencies and number of wavelengths in the system for the different situations is not physical: For $lcav = 0cm$ the frequency is 37046Hz and there are $\frac{17}{4}$ wavelengths in the system. For $lcav = 0.25cm$ the frequency is 37677Hz, but the number of wavelengths in the system are reduced to $\frac{15}{4}$. For $lcav = 0.33cm$ the frequency is 37726Hz, and the number of wavelengths are further reduced to $\frac{13}{4}$. At $lcav = 0.5cm$ the frequency is 37637Hz, and the wavelengths are back up to $\frac{15}{4}$. For $lcav = 0.67cm$ the frequency is 37532Hz with $\frac{17}{4}$ wavelengths in the system. Non of these changes in frequency and number of wavelengths are physically correct, and could indicate that the peak is not acoustic. However, as the pressure in the pipe for each case is acoustically valid, and the peak magnitude is increasing as the cavity length is increased (See figure 4.13(c))

the peak appears to be acoustic. As the peak not is zero for the case without a cavity, it's likely not excited by the cavity, but rather amplified by it. The theoretic frequencies for the number of wavelengths in the system are 13813Hz, 15938Hz and 18063Hz. This is 50% - 60% lower than the simulated frequencies.

The 5000Hz and 4th peak

The peaks between the 1st and the 2nd main peak are all of low magnitude. Of these small peaks, one with a clear acoustic pressure distribution is the peak at 5875Hz for the $lcav = 0.25cm$ case, and 5341Hz for the $lcav = 0.5cm$ case. The pressure curves for the 5000Hz peaks at the two cavity lengths looks very similar. The frequency on the other hand, is quite different. Physically, a change in frequency is the same thing as a change in wavelength. Like the case for the 3rd peak, this is not the case in this simulation and could suggest that the peak not is acoustic. The theoretic frequency for a smooth system would be 3187Hz. This is 37% and 46% lower than the simulated frequencies. Another peak excited by the cavity is the 4th peak. For $lcav = 0.25cm$, $lcav = 0.5cm$ and $lcav = 0.67cm$ this peak consists of $\frac{9}{4}$ wavelengths in the system. Theoretically this should give a 9562Hz frequency, which is 40% - 45% lower than the simulated frequencies. This peak is not present for $lcav = 0cm$, and increases as the cavity length is increased, except for $lcav = 0.67cm$. This reduction at the longest cavity length might be a result of phenomena regarding the specific frequency and the dimensions of the pipe. The increase in magnitude suggests that it's an acoustic peak.

Other peaks

Peaks with questionable acoustic relevance are plotted in appendix A.2. Here, the peaks at 3000Hz - 4000Hz and 35000Hz can be found. The 3000Hz-4000Hz peaks have very rough pressure curves, but can resemble half a wavelength in the pipe. This peak may, or may not, be acoustically relevant, and will not be discussed further.

5.1.2 Acoustics in Palabos

All the peaks with apparent acoustic behavior have a significantly lower frequency than theory would suggest. Some variation is expected as the space prior to the inlet, the flow and the cavity will have an influence on the system. Why the frequencies for the acoustic peaks are so far off the theoretic frequencies is unknown. Most peaks assumed to be acoustic in this simulation have different frequencies

for different cavity lengths. Small variations are excepted because of the geometry change. However, for acoustic peaks this change should be evident in the number of wavelengths in the pipe. For most cases of changed frequency, the change does not coincide with the pressure distribution in the pipe. The distribution is generally unchanged for the 1st main peak, the 4th and the 5000Hz peak, even though the frequencies are changing. The distribution is inconsistent for frequency changes for the 3rd peak. The reason for these changes in frequency and wavelengths could be that non of the peaks are acoustic. Other results however, like the close to 90° phase difference between pressure and particle velocity and the magnitudes of the peaks suggest that this is probably not the case. It's probably more an issue of simulating acoustics in Palabos. Palabos simulations very similar to the simulations conducted in this thesis has previously been done with more acoustically correct frequency results, [19]. In these previous simulations the pipe used was longer than in this thesis. This might play a part in the acoustic behavior of the simulation. Another uncertainty is the units used in Palabos. Unit conversion from LB to physical units is not straight forward, [20]. In order to calculate a physical frequency, both dimensionless units and LB units have to be calculated. Since the simulated frequencies are so far from the physical frequencies, the calculated sampling frequency seems questionable. If it's incorrect, a larger portion of the total frequency spectrum might have to be considered. The number of wavelengths in the pipe however, indicates that this is not the case. It's likely only a case of incorrect frequency labeling due to a too high sampling frequency. This might have something to do with the setting of a characteristic length (l_0), and how this choice affects the other parameters. For the simulations in this thesis, and in previous work [19], the characteristic length was set to $1cm$. As described in 3.1.1, the Reynolds number was reduced to 5800. What effect this reduction has on the simulation is unknown. Looking at the Reynolds number formula 2.4.1, a changed Reynolds number could change either the characteristic length, the velocity or the viscosity. If the characteristic length is changed, the size of the pipe is changed and the theoretic frequencies in table 3.1.1 would be incorrect. The acoustic effects of changing the Reynolds number, and acoustic simulations in Palabos in general needs to be studied further.

5.1.3 Instantaneous intensity

The instantaneous intensity at the downstream cavity edge is at a maximum when a cavity vortex just has left the cavity. The minimum instantaneous intensity is when a cavity vortex is about to hit the downstream cavity wall. Looking at figure 4.16, it's clear that the highest instantaneous intensity is in the cavity. The level in the inlet is higher than for the initial space, and the level in the downstream

portion of the pipe is higher than for the inlet. The levels are explained by the vortices as follows: The inlet vortices are the small, but elevates the level from the initial space. The cavity vortices are the most dominant, while the ones in the rest of the pipe are reduced versions of the vortices in the cavity. In a pipe either the pressure or the particle velocity is always zero at a pipe inlet or outlet. Therefore, the expected instantaneous intensity at these locations is zero. This is not the case in these simulations. The reason is likely the boundary conditions set in Palabos.

5.1.4 Inlet vortices

The concept of inlet vortices are explained in section 2.6.1 and 5.1. By studying the images in figure 4.18, and the inlet pressure and particle velocity in figure 4.17, the generation of inlet vortices can be investigated. To pinpoint exactly when the inlet vortices are created is not possible from these images, as the vortices not are well defined visually until they have traveled a certain distance down the pipe. However it's possible to give an estimate. It's believed that inlet vortices are generated at pressure maxima. To determine if this is the case is hard by studying the red and dark part of the pipe. This dark area is smeared out by the effects of the pipe flow and pulsation, and is not helpful until the vortices are halfway down the inlet. Looking at the lower velocity, blue area of the pipe, reveals that an even lighter blue area is emerging from the inlet edge (In the black circle). This happens at the pressure maximum, in figure 4.18(b), or the prior image in figure 4.18(a). In the images following, this blue area travels down the pipe. In image 4.18(e) and 4.18(m) the vortex appears to be more defined. This series of images of the velocity data indicates that the creation of inlet vortices is related to a pressure maximum at the inlet. It appears that a vortex at the inlet starts building prior to, and is released from the inlet after a pressure maximum. As a side note the pressure is leading the particle velocity. From figure 4.11 it can be seen that the phase difference is close to 90° between pressure and particle velocity, which is expected for acoustic waves.

5.2 Experiments

In this section the experimental results will be discussed. More specifically: The generation of inlet vortices. The sound pressure and power levels for the different pipe configurations. And possible cancellation of the whistling sound by adding a cancellation frequency.

5.2.1 Generated whistling sound and inlet vortices

The cavity lengths of which whistling sound were excited can be seen in section 4.2. When restarting the airflow in the attempt to excite whistling sounds for short cavity lengths, some peaks were excited at first, but then faded away. (See table 4.2.1.) These observations support the theory that the cavity vortices which generate the peaks, originally are created by inlet vortices. For short cavity lengths, when a fading peak is generated, the cavity vortices are not excited strongly enough, or of sufficient duration to create a significant pressure wave in the pipe. A pressure wave would stimulate the creation of inlet vortices after the initial unstable flow, and the whistling sound would not fade. When extending the cavity, the cavity vortices are increasing in magnitude and are able to stimulate the inlet vortices for a longer period of time. At a certain cavity length, the cavity vortices produce a strong enough pressure wave in the system to keep the generation of inlet vortices going. This theory is consistent with the simulation results discussed in section 5.1, as the inlet vortices for the situation without a cavity faded away. These explanations also coincide with [3], briefly explained in section 2.6.1. When increasing the cavity length to above approximately $10mm$, whistling frequencies would be excited even though the airflow was running and no whistling frequency was excited initially. This can appear contradictory to the latter discussion. An explanation can be that for long enough cavities, the cavity flow introduces an instability in the total pipe airflow, which causes the necessary conditions for inlet vortices to be generated.

5.2.2 Experimental measurements

Sound pressure level

Mode 1 was excited for two inlet lengths, $20mm$ and $25mm$, at approximately the same cavity lengths, $12mm$ - $21mm$. Mode 2 was excited most often. It's present for all inlet lengths except $20mm$, and varies in maximum sound pressure level. The highest maximum was for the case with no added inlet at $lcav = 11mm$ - $13mm$. The lowest maximum was for the case with a $30mm$ inlet at $lcav = 10mm$ - $13mm$. For all the three cases where mode 2 was the only dominant mode, a maximum sound pressure was excited for $lcav = 11mm$ - $13mm$. Mode 3 was excited at long cavity lengths for $10mm$ and $12mm$ inlet. It was the dominant mode only for the $20mm$ inlet at short cavity lengths, $lcav = 5mm$ - $10mm$. Maximum sound pressure in the pipe occured at $lcav = 8mm$. The longest inlet length was the most consistent regarding mode excitation and cavity length. For this inlet length mode 2 was excited from $lcav = 7mm$ - $21mm$. A $20mm$ inlet excited two distinct acoustic modes depending on the cavity length. The $25mm$ inlet could

excite two different acoustic modes for the same inlet length depending on a short duration boundary condition change at the inlet. The harmonics excited for the two situations are observed in figure 4.25. These observations does not provide any explanations on the physical phenomena.

Power

The maximum downstream power was generated by mode 1 with a $20mm$ inlet. The second highest power was also generated by mode 1. This time with a $25mm$ inlet. The power of mode 2 was one to three orders of magnitude lower than for mode 1 considering all inlet lengths. For a $25mm$ inlet, where both mode 1 and 2 were possible to excite, the difference was not as significant. The downstream power of mode 3 was insignificant. Generally, there was one downstream power peak per inlet length. For all situations there is a cavity range where the downstream power is at a peak. This peak is located in cavity length range $9mm$ - $15mm$. The upstream power data is calculated from a rougher approximation than the downstream power data, as described in section 2.2. This contributes to the less distinct appearance of the plots in figure 4.22. The largest difference in down- and upstream power was for mode 2, in the case without an added inlet. The smallest difference was for mode 1 with the $20mm$ inlet. There are also traces of more than one peak for situations with inlet length $12mm$ and $20mm$. Despite the roughness of the plots there are still clear tendencies towards that certain cavity lengths produce more upstream power than others. As the peak power cavity length is different for different inlet lengths, it's obvious that the inlet is causing this behavior. It's however not possible to say why this is from these limited number of measurements alone.

Dimenstionless power

The plots in figure 4.23 and 4.24 show the dimensionless power versus Strouhal number for one mode at the time. The magnitude of the dimensionless power is expected to be a number between 0 and 1, [12]. This is the case for most of the measurements, but in the case without added inlet the dimensionless power is a lot higher. Both for downstream and upstream power, the peak of mode 1 are close to $Sr = 0.2$. For upstream power at the $20mm$ inlet, there are two peaks, but the average of the two is close to 0.2, which satisfy $Sr_{opt} = 0.2$ for mode 1. For mode 2 and 3 the optimal Strouhal number is in the range $Sr_{opt} = 0.3$ - 0.4. This difference in Strouhal number from mode 1 indicates that a different hydrodynamic mode has been excited as the vortex velocity is up to 2 times higher, [7]. (See section 2.6.2.)

If this is the case, the 1st hydrodynamic mode is exciting the 1st acoustic mode, while the 2nd hydrodynamic mode is exciting the 2nd and 3rd acoustic mode. For the $25mm$ inlet, acoustic mode 1 and 2 can be excited at the same cavity lengths, implying that both hydrodynamic mode 1 and 2 are excitable for this inlet length. All excited acoustic frequencies are close to the frequency of a hydrodynamic mode.

5.2.3 Cancellation with added sound

The process of searching for cancellation frequencies are explained in section 5.2.3. For mode 1, only a small cancellation band was found. When searching in mode 2 no cancelation frequencies were found with $10mm$ and $25mm$ inlet length. Some cancellation frequencies were found for the $30mm$ inlet, while most were found for the $12mm$ inlet. (See table 4.2.2.) Note that an inlet extension of only $2mm$ changes the situation from no possible cancellation frequencies, to several cancellation frequency bands. The cancellation frequency bands can be seen in figure 4.25. Most of the frequencies affecting the whistling noise resulted in cancellation. In these bands the transition between whistling and dampening was gradual. For some frequencies, namely 730Hz and 1940Hz - 1980Hz the transition was instant. The frequency bands 1180Hz - 1377Hz and 2647Hz - 2700Hz did not quite cancel the whistling frequency, but disturbed it enough to make a permanent excitation impossible. The frequency band 1560Hz - 1700Hz cancelled mode 2 but excited mode 3. Searching in mode 3, only four cancellation bands were found. Of these bands the 3100Hz - 3450Hz did not quite cancel the whistling like two of the bands in mode 2. No connection is found when considering the cancellation frequency bands, acoustic modes of the pipe, hydrodynamic modes and inlet lengths. For this the cancellation bands are too wide, and the other variables too many. The level of the cancellation frequency at the measuring position was for most cases lower than the whistling sound. At most the difference was 16.5dB lower. If these cancellation levels are acceptable or not will depend on the application. As an aside there can be noted that in addition to the cancellation frequencies, pressure delta pulses at approximately 13Hz could cancel the whistling sound for all pipe configurations. Low frequency cancellation is discussed for corrugated pipes in [17].

Chapter 6

Conclusion

The experimental measurements show that pipe modes are excited for a variety of cavity lengths. In these situations with a constant flow velocity, the inlet and cavity lengths decide the pipe mode excited. The whistling frequencies with most power are generated at Strouhal number 0.2 and 0.4, for acoustic mode 1 and 2. Acoustic mode 1 is excited by hydrodynamic mode 1 and acoustic mode 2 and 3 are excited by hydrodynamic mode 2. Cancellation of the whistling sound is possible for certain modes and inlet lengths. Unfortunately, a pattern in the cancellation frequency bands has not been found. It's interesting to observe that a $2mm$ difference in inlet length changes the possible cancellation frequency bands from zero to several. A Palabos simulation of these scenarios could give a visual insight to what causes this behavior, and is recommended for future studies. The fading inlet vortices from the simulation without a cavity, and the whistling behavior at short cavity lengths in the experiments point towards the necessity of inlet vortices for hydrodynamic and acoustic modes to be excited.

The simulation results show that a single cavity in a pipe excites acoustic peaks. For the fundamental mode the peak magnitude increases with increased cavity length. For the $lcav = 0.5cm$ case the hydrodynamic and acoustic modes have the same frequency, and the pressure and particle velocity is close to 90° out of phase. The visual representation of the simulation provides a way of understanding the behavior of the vortices in the system. The simulations have shown that Palabos can be used to simulate acoustic waves in a pipe-cavity system. It's important to analyze the results in order to understand which frequency peaks are acoustic and which are not. The frequency peaks measured in this thesis are not in accordance with the physically expected modes of the simulated pipe. The expected frequencies

are 40° - 60° lower than the measured frequencies, which is a substantial deviation. This deviation is probably a result of incorrect sampling frequency calculations. A change in frequency, and corresponding change in wavelengths for a specific frequency peak, is also not physically correct as a higher frequency dictates more wavelengths in the pipe. This is the main point not in favor of using Palabos for acoustic simulations. As this software has been used with more success in the past, and the pressure, phase and magnitude results seem to be acoustically valid, the conclusion is that Palabos is a promising software for acoustic simulations. However further work needs to investigate how to correctly find the acoustic peaks, the sampling frequency and what effects a change of Reynolds number has on the simulations. Also, a more detailed visual representation of the inlet and cavity could prove interesting because it would give a better view of the vortices.

Bibliography

[1] Forskningsrådet. URL *http://www.forskningsradet.no/servlet/Satellite?c=Nyhet&pagename=petromaks%2FHovedsidemal&cid=1226993731411&p=1226993690946*.

[2] Daniel Mazzoni and Ulf Kristiansen. *Aero acoustics of a flow pipe having a single small cavity.* Forum Acousticum , Aalborg Denmark. European Acoustics Association, 2011.

[3] Ulf R. Kristiansen and Geir A. Wiik. *Experiments on sound generation in corrugated pipes with flow.* Journal Acoustical Society of America 121 (3), March 2007.

[4] Dr. Hugh Goyder. *On the modelling of noise generation in corrugated pipes.* Proceedings of the ASME 2009 Pressure Vessels and Piping Division ConfeDreRnAceF, July 2009.

[5] R. Swindell andBureau Veritasand S. Belfroid. *Internal Flow Induced Pulsation of Flexible Risers.* TNO TPD, Offshore Technology Conference, 2007.

[6] V.Debut, J. Antunes, and M.Moreira. *Flow-acoustic interaction in corrugated pipes: Time-domainsimulation of experimental phenomena.* Institude of Thermomechanics, Prague, 2008.

[7] Devis Tonon, Avraham Hirschberg, Joachim Golliard, and Samir Ziada. *Aeroacoustics of pipe systems Aeroacoustics of pipe systems with closed branches.* Eindhoven University of Technology, Fluid Dynamics Laboratory and TNO Science and Industry, Delft, The Netherlands and McMaster University, Department of Mechanical Engineering, Hamilton, Ontario.

[8] Lawrence E. Kinsler Austin R. Frey Alan B. Coppens James V. Sanders. *Fundamentals of Acoustics.* John Wiley & Sons, Inc., 2000.

[9] Wikipedia.org: Acoustic waves, . URL *http://en.wikipedia.org/wiki/Acoustic_wave*.

[10] Wikipedia.org: Reynolds number, . URL *http://en.wikipedia.org/wiki/Reynolds_number*.

[11] Wikipedia.org: Strouhal number, . URL *http://en.wikipedia.org/wiki/Strouhal_number*.

[12] Güneş Nakiboğlu. *Aeroacoustics of corrugated pipes*. PhD thesis, Eindhoven University of Technology, 2012.

[13] Ulf R. Kristiansen and Erlend M. Viggen. *Computional Methods in Acoustics*. Norwegian University of Science and Technology.

[14] Wikipedia.org: Laminar flow, . URL *http://en.wikipedia.org/wiki/Laminar_flow*.

[15] Wikipedia.org: Turbulent flow, . URL *http://en.wikipedia.org/wiki/Turbulence*.

[16] Ulf Kristiansen, Daniel Mazzoni, and Anders Bakke Krogvig. *Aeroacoustic investigation of a one-cavity flowpipe using the Lattice Boltzmann method*. The 35th Scandinavian Symposium on Physical Acoustics, January 2012.

[17] Ulf R. Kristiansen, Pierre-Olivier Mattei, Cedric Pinhede, and Muriel Amielh. *Experimental study of the influence of low frequency flow modulation on the whistling behavior of a corrugated pipe*. Journal Acoustical Society of America 130 (4), October, 2011.

[18] The palabos project. URL *http://www.palabos.org/*.

[19] Daniel Mazzoni. Acoustics in lattice boltzmann simulations. Technical report, Ecole Centrale Marseille Technopôle de Château-Gombert.

[20] Jonas Latt. *Choice of units in lattice Boltzmann simulations*. The Palabos open source project, www.palabos.org, April 2008.

Appendix A

Simulation

A.1 Calculation of physical sizes

These calculations are based on [19] and [20]. The following subscripts are used:
d - dimensionless
p - physical
0 - characteristic
s - sampling

Reynolds number

$Re = \frac{ud}{w} = \frac{10ms^{-1}0.01m}{0.000015m^2s^{-1}} = \underline{6667}$

Physical length

L - length
H - height

$L_{d,system} = 2000$
$L_{d,pipe} = 1500$
$H_d = 500$

$L_0 = 1cm$, the characteristic length, is the pipe diameter. $L_{0,d} = 250$. Therefore, the dimensions of the system are:

$L_p = \frac{L_d}{250}$

$L_{p,system} = \frac{2000}{250} = \underline{8cm}$

The length of the pipe is:
$L_{p,pipe} = \frac{1500}{250} = \underline{6cm}$

The height of the system is:
$H_{p,system} = \frac{500}{250} = \underline{2cm}$

The height of the pipe is:
$H_{p,system} = \frac{250}{250} = \underline{1cm}$

Physical sampling frequency

$f_d = \frac{f_p}{f_0}$

$f_0 = \frac{1}{t_0}$

$t_0 = \frac{L_0}{v_0}$, $L_0 = 1cm$, $v_0 = 10\frac{m}{s}$

$t_0 = \frac{0.01}{10} = \frac{1}{1000}$

$f_0 = \frac{1}{\frac{1}{1000}} = \underline{1000}$

$f_{s,d} = \frac{1}{t_d} = \frac{1}{1000} = \underline{1000}$

$f_{s,p} = f_{s,d} f_0$

$f_{s,p} = 10001000 = \underline{1000000Hz}$

A.2 Simulated frequency peak with questionable acoustic relevance

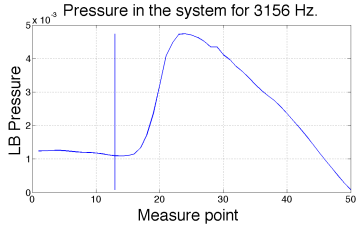

(a) 3156Hz

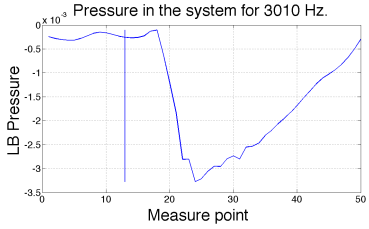

(b) 3010Hz

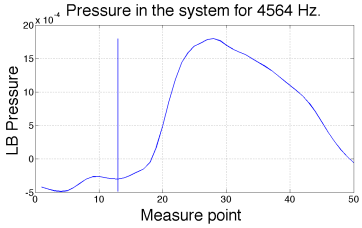

(c) 4564Hz

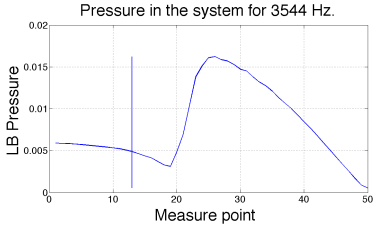

(d) 3544

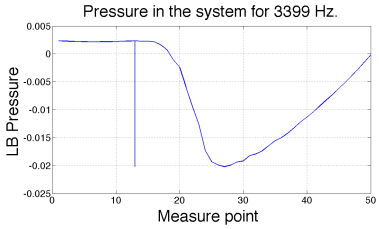

(e) 3399Hz

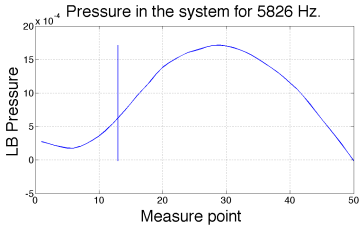

(f) 5826Hz

Figure A.1: Peaks between 3000 - 6000Hz

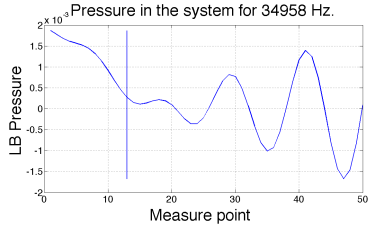

(a) 34958Hz Hz

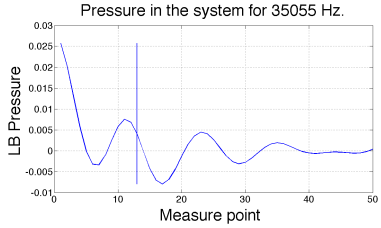

(b) 35055 Hz

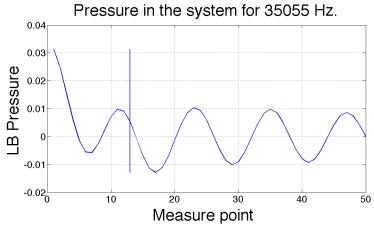

(c) 35055 Hz

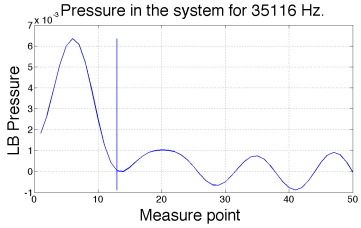

(d) 35116 Hz

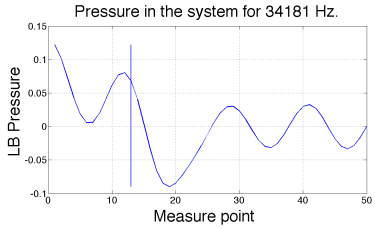

(e) 34181 Hz

Figure A.2: The 35000Hz peak

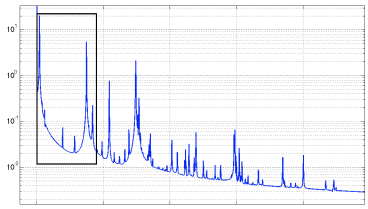

Figure A.3: Total frequency spectrum from simulation $lcav = 0.5cm$. Black Square: Area discussed in this thesis

Appendix B

Experiments

B.1 Experimental equipment

The experimental equipment:
• Acoustic filter: Wavetek Dual mode HI LO Filter model 442.
• Microphone: Norsonic, Norsonic front end type 336.
• Velocimeter: ALNOR model 560.
• Voltmeter: Metric Bruel & Kjaer type 2409.
• Amplifier: adyton xp1.
• Frequecy generator: Wavetek Model 135, LIN/LOG sweep generator.
• Loudspeaker driver: JBL GT5 - 1.
• Regular vacuum cleaner with hose.
• Wooden box [cm]: L x W x H: 57 x 29 x 32.5 .
• Pipe/cavity geometry: See section 3.2.1.

B.2 Calculation of end correction

$L_{corr} = \frac{8 \cdot 0.043}{2 \cdot 3\pi} + 0.6 \cdot \frac{0.043}{2} = 0.031$

Shortest pipe configuration: $L_{eff} = 0.660 + L_{corr} = \underline{0.691}$
Longest pipe configuration: $L_{eff} = 0.700 + L_{corr} = \underline{0.731}$

B.3 Frequencies measured

Inlet length = 10mm

lcav (mm)	Frequency (Hz)
1	0
2	0
3	0
4	0
5	0
6	0
7	0
8	0
9	0
10	0
11	485
12	483
13	482
14	481
15	479
16	478
17	477
18	476
19	475
20	473
21	718

(a) 0mm added inlet

Inlet length = 12mm

lcav (mm)	Frequency (Hz)
1	0
2	0
3	0
4	0
5	0
6	483
7	481
8	479
9	478
10	476
11	475
12	474
13	473
14	472
15	471
16	469
17	466
18	720
19	716
20	711
21	0

(b) 2mm added inlet

Inlet length = 20mm

lcav (mm)	Frequency (Hz)
1	0
2	0
3	0
4	0
5	722
6	719
7	716
8	714
9	711
10	708
11	238
12	236
13	235
14	234
15	233
16	233
17	232
18	232
19	231
20	231
21	230

(c) 10mm added inlet

Inlet length = 25mm

lcav (mm)	Frequency (Hz)
1	0
2	0
3	0
4	0
5	0
6	0
7	0
8	0
9	0
10	0
11	234
12	233
13	232
13	477
14	231
14	475
15	231
15	474
16	230
16	472
17	229
17	471
18	228
18	470
19	228
19	469
20	227
20	468
21	0
21	468

(d) 15mm added inlet

Inlet length = 30mm

lcav (mm)	Frequency (Hz)
1	0
2	0
3	0
4	0
5	0
6	0
7	472
8	471
9	469
10	468
11	467
12	466
13	464
14	463
15	462
16	461
17	459
18	459
19	458
20	457
21	456

(e) 20mm added inlet

Figure B.1: The frequencies measured for different inlet lengths.

B.4 Additional experimental measurements and data

Minimum sound pressure inside the pipe was measured in order to calculate intensity and power.

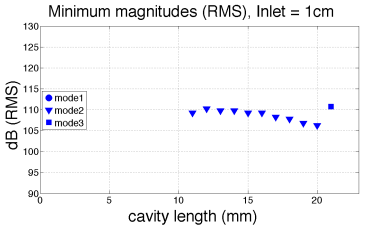

(a) Inlet length: 10mm

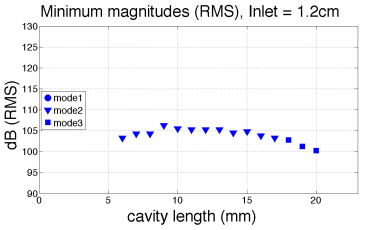

(b) Inlet length: 12mm

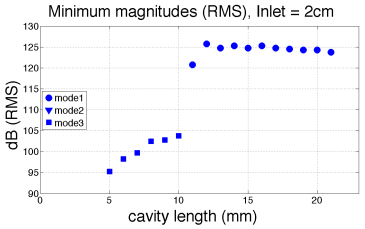

(c) Inlet length: 20mm

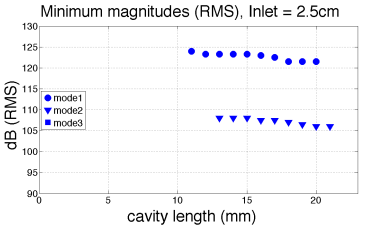

(d) Inlet length: 25mm

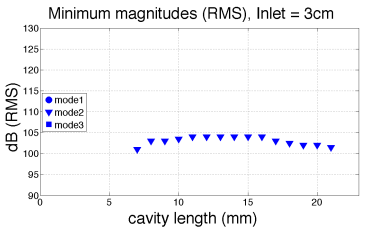

(e) Inlet length: 30mm

Figure B.2: Minimum sound pressure level in the pipe

Comments: Minimum pressure nodes
The minimum levels are measured at pressure nodes where the pressure is supposed to be zero. These measurements are hard to execute because the nodes are very location specific. The output signal from the filter had a bandwidth of 20-30Hz, and will therefore let more than one frequency through.The minimum levels measured were not zero, but versus cavity length the curve is fairly flat. This was expected

as the pressure in theory is zero.

Sound pressure outside the pipe was measured on axis, 15cm from the pipe inlet, in order to calculate upstream intensity and power.

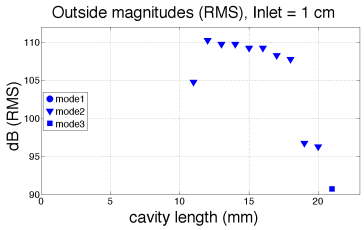

(a) Inlet length: 10mm

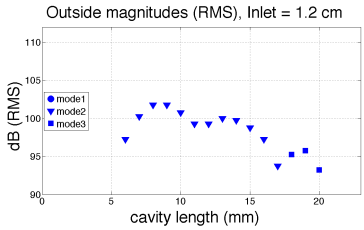

(b) Inlet length: 12mm

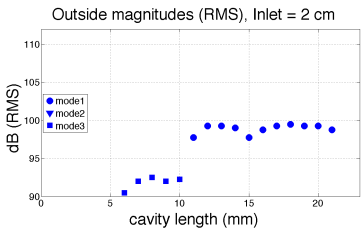

(c) Inlet length: 20mm

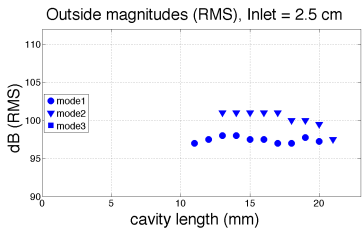

(d) Inlet length: 25mm

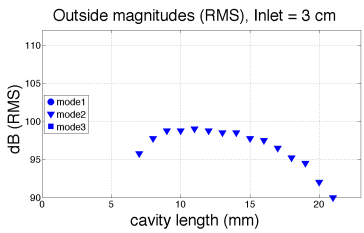

(e) Inlet length: 30mm

Figure B.3: Sound pressure level outside the pipe

The upstream and downstream intensity was calculated by using theory from section 2.2.

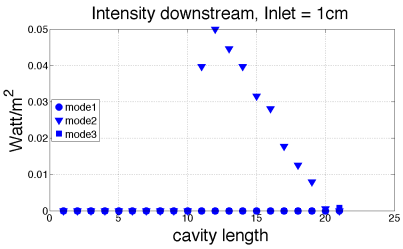

(a) Inlet length: 10mm

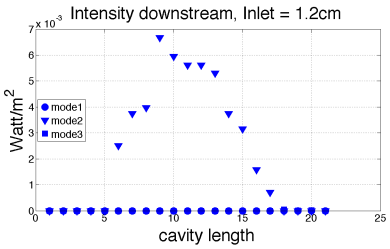

(b) Inlet length: 12mm

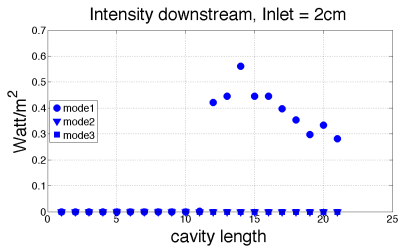

(c) Inlet length: 20mm

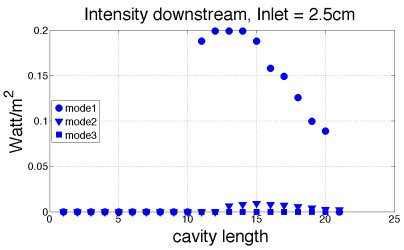

(d) Inlet length: 25mm

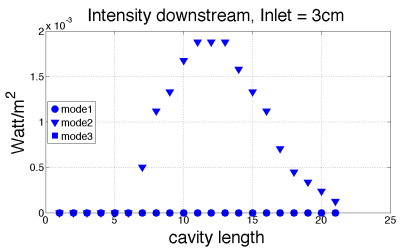

(e) Inlet length: 30mm

Figure B.4: Net intensity downstream (RMS)

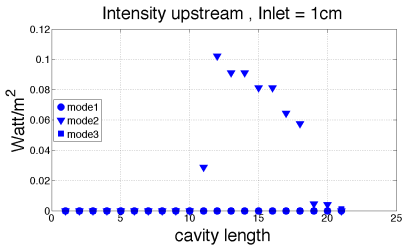

(a) Inlet length: 10mm

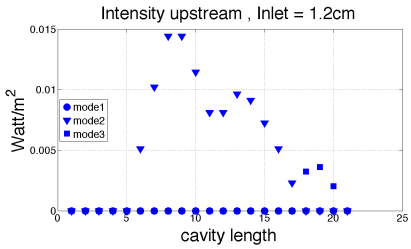

(b) Inlet length: 12mm

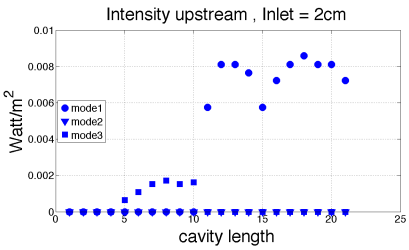

(c) Inlet length: 20mm

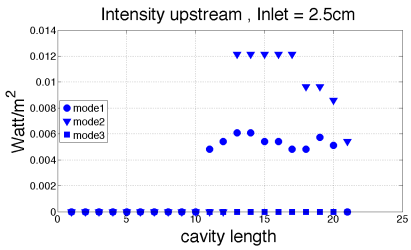

(d) Inlet length: 25mm

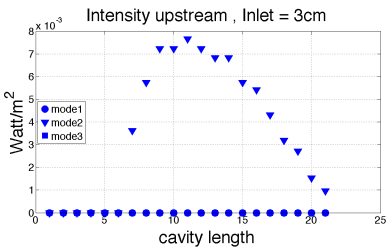

(e) Inlet length: 30mm

Figure B.5: Intensity upstream (RMS)